NUREG/CR-0832
ORNL/NUREG/CSD/TM-8

INCAP: A Finite Element Program for One-Dimensional Nonlinear Inverse Heat Conduction Analysis

B. R. Bass

Prepared for the U.S. Nuclear Regulatory Commission
Office of Nuclear Regulatory Research
Under Interagency Agreements DOE 40-551-75 and 40-552-75

OAK RIDGE NATIONAL LABORATORY
OPERATED BY UNION CARBIDE CORPORATION · FOR THE DEPARTMENT OF ENERGY

Printed in the United States of America. Available from
National Technical Information Service
U.S. Department of Commerce
5285 Port Royal Road, Springfield, Virginia 22161

NUREG/CR-0832
ORNL/NUREG/CSD/TM-8
Dist. Category R2

Contract No. W-7405 eng 26

Computer Sciences Division

INCAP: A FINITE ELEMENT PROGRAM FOR ONE-DIMENSIONAL NONLINEAR INVERSE HEAT CONDUCTION ANALYSIS

(Sponsor: J. D. White; Originator: B. R. Bass)

B. R. Bass

Computer Sciences Division

Manuscript Completed - April 1979
Date Published - July 1979

Prepared for
Office of Nuclear Regulatory Research
U. S. Nuclear Regulatory Commission
Washington, DC 20555
Under Interagency Agreements DOE 40-551-75 and 40-552-75

NRC FIN No. B0125

UNION CARBIDE CORPORATION, NUCLEAR DIVISION
operating the
Oak Ridge Gaseous Diffusion Plant . Oak Ridge National Laboratory
Oak Ridge Y-12 Plant . Paducah Gaseous Diffusion Plant
for the
DEPARTMENT OF ENERGY

TABLE OF CONTENTS

ACKNOWLEDGMENTS

This study was supported by the Nuclear Regulatory Commission through the Oak Ridge National Laboratory Pressurized-Water Reactor Blowdown Heat Transfer Separate-Effects Program. The author appreciates the contributions made by R. A. Hedrick and L. J. Ott of ORNL.

LIST OF FIGURES

LIST OF FIGURES (Contd.)

LIST OF SYMBOLS

Symbol	Definition
a	Radius of cylindrical rod
$[B]$	Matrix, as defined in equation (10)
$[C]$	Heat capacity matrix for assembly of elements
C_i	Thermal expansion coefficients in gap width model, equation (32)
c	Specific heat
e	Index of elements
E	Number of elements in assembly
$\{\bar{F}\}$	Vector for assembly of elements, equation (11)
$\{\bar{\bar{F}}\}$	Vector for assembly of elements, equation (12)
h	Convective heat transfer coefficient
h^r	Radiative heat transfer coefficient, equation (5)
J	Number of time steps in analysis interval; J - 1 equals number of "future" temperatures
$[K]$	Thermal conductivity matrix for assembly of elements
k	Thermal conductivity
L	Distance of temperature probe from surface of body
M	Number of nodes
N_I	Interpolation function
$\{N\}$	Vector of interpolation functions
$\underline{n}$	Unit outward normal to boundary surface
Q	Internal heat generation rate, per unit volume
q	Imposed surface heat flux
q^c	Surface heat flux due to convection
q^r	Surface heat flux due to radiation

LIST OF SYMBOLS (Contd.)

Symbol	Definition
r	Radial coordinates, one-dimensional model
r_I	Radial coordinates of node point I
r^p	Radial coordinate of temperature probe location
Δr_{gap}	Width of sheath gap in heater rod model, equation (32)
r_{15}	Inner radius of sheath gap interface, equation (32)
r_{16}	Outer radius of sheath gap interface, equation (32)
$[S]$	Matrix, as defined in equation (16)
T	Temperature
T_I	Value of temperature at Ith node
$\{T\}$	Temperature vector
T^p	Measured temperature at internal point r^p of body
T^{ac}	Temperature at which no convection occurs
T^{ar}	Temperature at which no radiation occurs
T^w	Temperature at wall
T_{av}	Computed temperature at thermocouple probe position r^p averaged over analysis interval, equation (31)
T^p_{av}	Input temperature at thermocouple probe position r^p averaged over analysis interval, equation (31)
T_{15}	Computed temperature at inner surface of sheath gap interface in heater rod model, equation (32)
T_{16}	Computed temperature at outer surface of sheath gap interface in heater rod model, equation (32)
t	Time
TOL1	Convergence tolerance, equation (18)
TOL2	Tolerance for temperature error, equation (30)

LIST OF SYMBOLS (Contd.)

Symbol	Definition
W	Summed weights function, equation (31)
w_j	Weighting functions, equation (27)
$\underline{x}$	General spatial coordinates

Greek Symbols	Definition
α	Thermal diffusivity
ρ	Density
Ω	General spatial domain
Ω^e	Element domain
Γ_1	Boundary on which condition (2) is prescribed
Γ_2	Boundary on which condition (3) is prescribed
$\Gamma_2{}^e$	Element external boundary on which condition (3) is prescribed
∇	Gradient operator
σ	Stefan-Boltzmann constant
ϵ	Emissivity
η	One-dimensional coordinate of parent element
β	Surface heat flux parameter, equation (26)
Δ	Incremental change in kernel
τ	Dimensionless time
Σ	Summation symbol

LIST OF SYMBOLS (Contd.)

Subscripts	Definition
I	Index of nodes
i	Index of time steps in solution, where i is a non-negative integer
j	Index of time steps in analysis interval, $1 \leq j \leq J$
$(i)\Delta t$	Time $t = (i)\Delta t$ at which kernel is evaluated

Superscripts	Definition
$[\ ]^T$	Transpose of matrix
$\{\ \}^T$	Row vector
(P)	Iteration number at which kernel is evaluated

Other Symbols	Definition
$[\ ]$	Matrix
$\{\ \}$	Column vector
$\|\|\ \|\|$	Euclidean norm
$\int$	Integral sign

INCAP: A FINITE ELEMENT PROGRAM FOR ONE-DIMENSIONAL NONLINEAR INVERSE HEAT CONDUCTION ANALYSIS

B. R. Bass

ABSTRACT

The calculation of the surface temperature and surface heat flux from a measured temperature history at an interior point of a body is identified in the literature as the inverse heat conduction problem. This report presents apparently the first application of an inverse solution technique that utilizes a finite element heat conduction model and Beck's nonlinear estimation procedure. The technique is applicable to the one-dimensional nonlinear model with temperature-dependent thermophysical properties. A digital computer program INCAP (INverse Heat Conduction Analysis Program) is developed from the formulation and is used in a comparative study with the finite difference inverse code ORINC (ORNL INverse Code). Specifically, two representative thermocouple transients obtained from electrically heated composite rods during a simulated loss-of-coolant accident are analyzed with INCAP and ORINC and the results are compared.

I. INTRODUCTION

The Oak Ridge National Laboratory (ORNL) Pressurized-Water-Reactor Blowdown Heat Transfer (PWR-BDHT) Separate-Effects Program [1] is part of the overall light-water-reactor (LWR) safety research program of the Nuclear Regulatory Commission (NRC). Other parts of the program cover a wide range of experimental and analytical efforts, from laboratory to small-scale experimental nuclear plants; the separate-effects studies, which fall between these two, are designed to answer specific questions relevant to the hypothetical loss-of-coolant accident (LOCA).

Specific objectives of the ORNL PWR-BDHT Separate-Effects Program are to determine, for a wide range of parameters, time to CHF (critical heat flux) and the following variables for both pre- and post-CHF: heat fluxes, ΔT (temperature difference between pin surface and fluid), heat transfer coefficients, and local fluid properties. The program also seeks to test the ability of existing codes, such as RELAP [2], to predict the behavior of the single-rod and 49-rod loops under blowdown conditions.

The parameters to be studied include

1. Single and double-ended coolant line breaks of varying area ratios;
2. Fast to slow depressurization rates;
3. Combinations of system power and pressure to obtain different values of the departure from nuclear boiling ratio (DNBR);
4. A range of power cutoff delays;
5. A range of power decay rates;
6. A range of power-to-system volume ratios.

Secondary objectives are (1) to obtain CHF data under steady-state conditions over a range of coolant pressures, inlet and exit subcooling, and an inlet flow rate appropriate to PWR interests; (2) to evaluate the thermal-hydraulic behavior of the test loops during simulated operational upsets that include variations in local power, system pressure, or coolant flow using the anticipated transient without scram (ATWS) [3] as a guide; and (3) to determine the effect of different spacer grids and power distribution profiles on both transient and steady-state CHF.

II. TEST FACILITIES

Primary test results are obtained from the Thermal-Hydraulic Test Facility (THTF) [1], a large nonnuclear experimental loop with a test section that contains a 7 x 7 array of 12-ft heater rods with an outside diameter of 0.422 in. and a stepped, chopped-cosine power profile.

A schematic view of the THTF is shown in Figure 1. Fluid discharged from the pump flows through two control valves, where excess pump head is dissipated and flow adjusted to the desired level by diverting a portion through the bypass line. Heat generated in the fluid by the pump is removed in the small Graham "Heliflow" heat exchanger in the bypass line. The primary flow then passes through inlet instrumented spool pieces 1 and 2, where flow conditions are monitored by a combination of a drag disk, gamma densitometer, turbine meter, and temperature and pressure sensors in each spool piece. Flow enters the test section at the top of the rectangular shroud box, flows down its length, and enters the bottom of the rod bundle. The fluid exits the bundle through outlet spool pieces 1 and 2, which are identical to those on the inlet. The energy added by the test section header rods is removed by Graham "Heliflow" heat exchangers A, B, and C. Finally, the fluid returns to the pump section past the line from the pressurizer, which provides the primary pressure control for the loop and at the same time serves as a surge tank.

At the instant of blowdown, the contents of the primary loop may be discharged through either of two rupture disk assemblies and appropriately sized orifices into the pressure-suppression system. For approximately 15 sec before and approximately 300 sec after blowdown, over 500 sensors

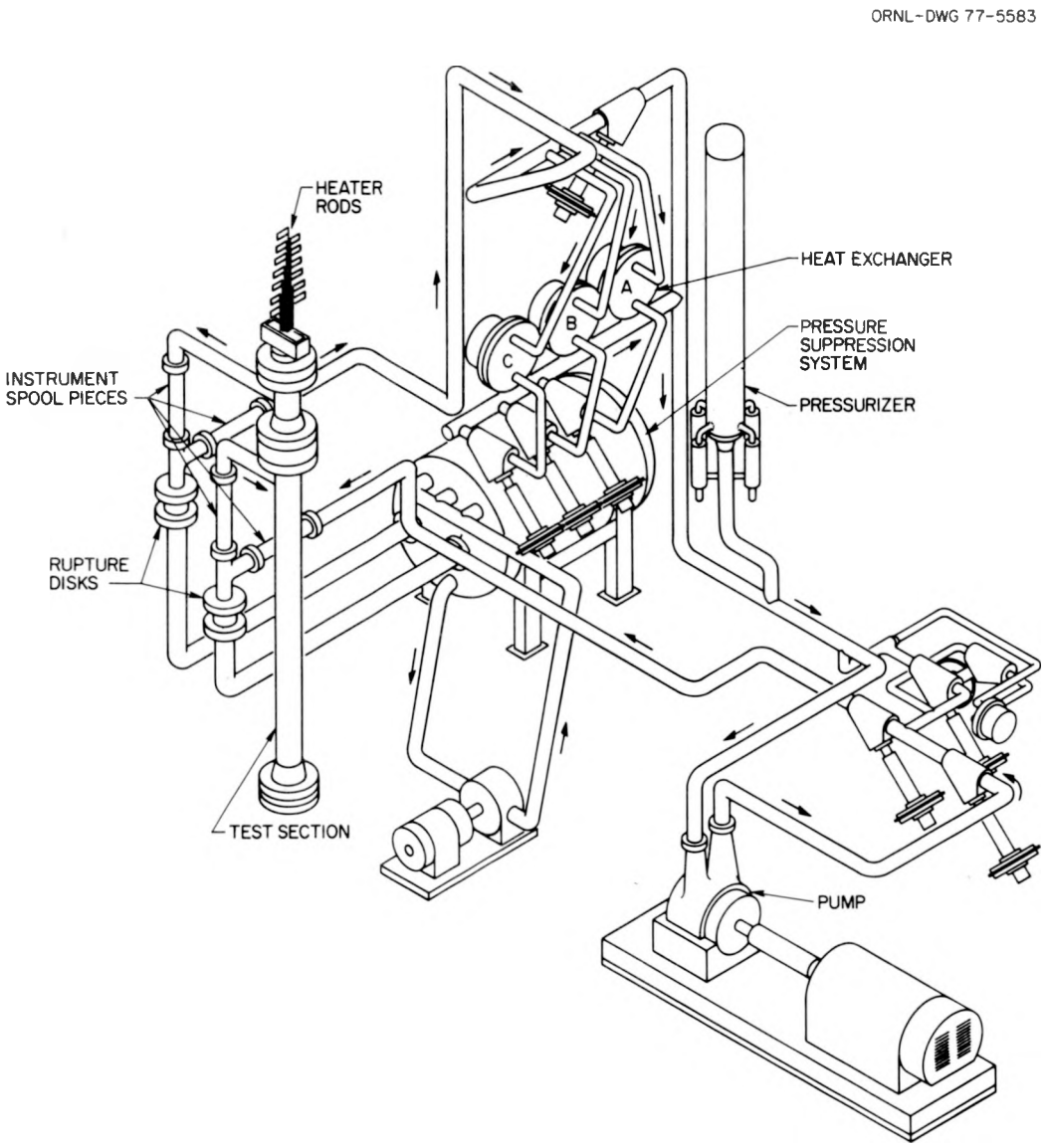

Figure 1. Thermal-Hydraulic Test Facility (ORNL-PWR Blowdown Heat Transfer Separate-Effects Program)

throughout the loop will be scanned by a computer-controlled digital-data-acquisition system (CCDAS) at a rate of 20 times per second. These sensors include approximately 320 thermocouples in the heater rods of the test section.

Supporting experiments are carried out in the Forced Convection Test Facility (FCTF). A schematic view of the principal FCTF loop components is illustrated in Figure 2. The primary purpose of the FCTF is to qualify prototype heaters for use in the THTF and to obtain blowdown heat transfer and steady-state CHF results for single rods in an annular geometry. In its present configuration, the FCTF is capable of conducting only single-ended break tests.

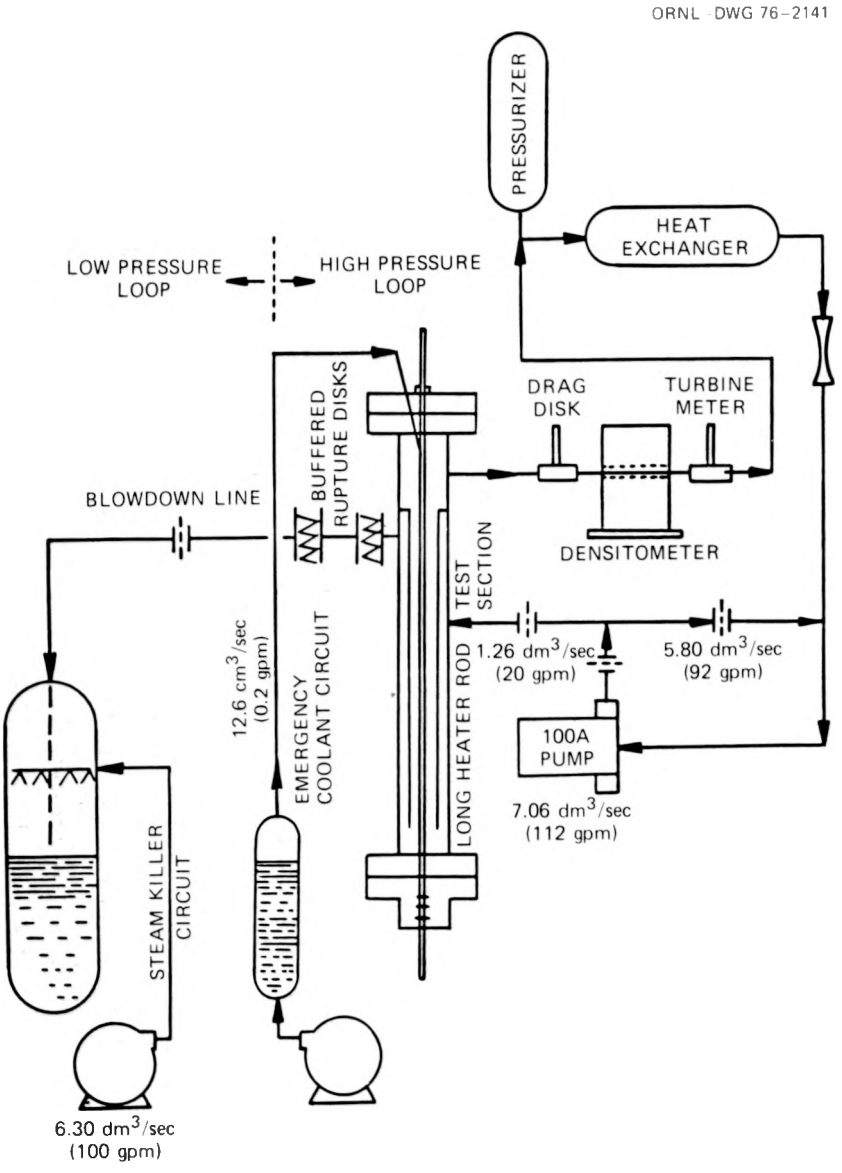

Figure 2. Forced Convection Depressurization Loop

III. OBJECTIVE

A primary objective of the PWR-BDHT Separate Effects program is to determine the transient surface temperature and surface heat flux of the THTF heater rods from internal temperature histories recorded during a blowdown. This necessitates solving the inverse heat conduction problem, where unknown boundary conditions are computed from known thermal responses measured internal to the body. To meet this objective, Ott and Hedrick [4] developed a one-dimensional, implicit finite difference formulation of the inverse problem. Ott and Hedrick implemented this formulation in the digital computer program ORINC (ORNL INverse Code) which performs the inverse calculation at rod thermocouple positions in the THTF bundle.

The validation process for ORINC is made difficult by the lack of any experimental data with which to compare directly the ORINC inverse calculations. As a partial solution to this problem, an alternate formulation of the nonlinear transient inverse problem is developed in this report and then used in a comparative study with ORINC. This formulation is based on finite element analysis and Beck's second method [5] and is applied in the digital computer code INCAP (INverse Heat Conduction Analysis Program). For a one-dimensional model of an actual heater rod-thermocouple configuration, two test cases are examined to assess the ability of INCAP to track rapid transients typical of a blowdown. Comparisons are then made between ORINC and INCAP for representative thermocouple transients at two thermocouple positions in the THTF bundle.

IV. A SURVEY OF PREVIOUS WORK

In transient heat conduction analysis, a class of problems can be identified where the temperature history is known at some interior point in the body and the transient surface temperature and surface heat flux are to be determined. This class is generally referred to in the literature as the inverse problem, in contrast with the usual direct formulation where the interior temperature history is determined from specified boundary conditions. Typically, the inverse formulation arises in experimental studies where direct measurement of surface conditions is not feasible, such as convective heat transfer in rocket nozzles and quenching of solids in a fluid. One application examined in this paper deals with two-phase flow over the surface of an electrically-heated rod that contains thermocouple probes in the interior.

Various solution methods have been applied to the inverse problem over the past two decades, including integral equation solutions, series solutions, transform solutions, and function minimization techniques. In one of the earliest papers, Stolz [6] obtained a linear solution by numerical inversion of the integral solution of the direct problem. His solution was found to be unstable for small time steps. Using an integral approach similar to that of Stolz, Beck [7] utilized a least squares technique to generate solutions for a much smaller time step. In a recent paper, Arledge, et al [8] also use an integral solution procedure which is valid for constant thermal properties. Burggraf [9] devised a series solution to the linear inverse problem which is exact only for continuous input data. Makhin and Shmukin [10], Kover'yanov [11], Plummer, et al [12], and Mehta [13] also utilize a series solution. Sparrow, et al [14] and

Imber and Khan [15] apply the transform method to the linear problem. Imber [16] has developed a transform solution to the inverse problem that is applicable to two-dimensional bodies of arbitrary shape when input data are known at suitable interior locations. In all of these papers, linearity of the model is essential to the formulation.

Several references consider the nonlinear problem of analyzing a composite body with temperature-dependent thermal properties. Ott and Hedrick [4] have developed a one-dimensional, implicit finite difference formulation and have applied it to an electrically-heated composite rod with temperature-dependent geometry and material properties. Beck has examined the nonlinear problem using a finite difference method [17] that builds on the ideas in Reference [7] and, more recently in Reference [5], has incorporated his function minimization technique into the framework of nonlinear estimation. Important to Beck's "second" method [5] is the observation that the temperature response at an interior location is delayed and damped with respect to changes in surface conditions. Beck, therefore, determines the surface heat flux in a given time step with a procedure that utilizes interior temperature data at "future" times. The surface heat flux is assumed to be a constant or low order polynomial over an analysis interval that consists of several time steps in the discretized data. The coefficients that describe the heat flux are adjusted iteratively to achieve the closest agreement in a least squares sense with the input "future" temperatures over the analysis interval. Less flexible versions of Beck's technique were considered earlier by Frank [18] and Davies [19]. Muzzy, et al [20] have adapted Beck's second method, with some modifications, into an explicit finite difference scheme for one-dimensional composite bodies with temperature-dependent material properties.

The finite difference method has been the predominant numerical technique for solution of the direct problem of heat conduction, and is applied in the nonlinear inverse formulations of References [4], [5], [17], and [20]. In recent years, the finite element method [21] has become well established as another numerical technique for heat conduction analysis. The finite element approach has demonstrated great versatility in modeling homogeneous or composite bodies with temperature-dependent material properties and complex geometries and boundary conditions. (See, for example, References [22], [23], [24].) In addition to these benefits, the technique shows considerable promise for the solution of coupled heat conduction and thermal stress problems [25,26].

In a recent paper, Hore, et al [27] present what is evidently the first application of the finite element method to the inverse problem. They develop a procedure for determining the surface heat flux at one boundary of a one-dimensional linear system from a known temperature history at an interior point. An iterative technique is used to determine incremental changes in surface heat flux until the error in the computed temperature at the interior point is within a prescribed tolerance. In their analysis, the surface flux is evaluated using contemporary input temperatures only, i.e., no "future" temperatures are utilized to determine surface flux as in Beck's second method.

In Reference [27], the finite element formulation of the inverse problem is applied to two numerical examples with known solutions. The first example treated is that of a constant heat flux imposed on the surface, while the second considers a periodic square wave heat flux. For both cases, the predicted temperature at the interior node closely

followed the input temperature values. However, the two examples exhibited numerical instabilities for the heat flux calculations, in the form of oscillations that progressively diverged in time from the known heat flux solution. Hore, et al identify some other difficulties with their inverse solution technique, including that of using temperature data measured at points far removed from the surface to solve for the surface heat flux. A potential difficulty with their technique is that it does not minimize the effect of experimental errors incurred in the temperature measurements at interior points. When these data are not smooth, oscillations in the calculated values of the heat flux can result. Hore, et al speculate that the nonlinear estimation techniques of Beck, along with the use of "future" temperatures, could possibly alleviate some of these difficulties.

The inverse solution technique described in the following sections and implemented in the digital computer code INCAP represents, to the author's knowledge, the first application of Beck's nonlinear estimation procedure in a computational scheme based on a finite element model of the direct problem. Discussion of the finite element formulation and Beck's procedure is followed by application of this inverse technique to four problems. First, two numerical examples with known solutions are treated to evaluate the performance of the technique in solving the inverse problem. Finally, the technique is applied to two experimentally determined temperature transients taken from interior points of an electrically-heated composite rod. The finite element computations from INCAP are compared with the results obtained by applying the finite difference inverse code ORINC to the same data.

V. FINITE ELEMENT FORMULATION OF THE DIRECT PROBLEM

The conduction of heat in the region Ω is governed by the quasi-linear parabolic equation

$$\nabla \cdot (k\nabla T) + Q = \rho c \frac{\partial T}{\partial t} \tag{1}$$

subject to the boundary conditions

$$T = T^{w} \text{ on } \Gamma_1 \tag{2}$$

and

$$k\nabla T \cdot \underline{n} + q + q^{r} + q^{c} = 0 \text{ on } \Gamma_2 \tag{3}$$

The heat flow rates per unit area on convection and radiation boundaries are written

$$q^{c} = h(T - T^{ac}) \ , \quad q^{r} = h^{r}(T - T^{ar}) \ , \tag{4}$$

where h^{r} is defined by

$$h^{r} = \varepsilon\sigma(T^2 + T^{ar^2})\ (T + T^{ar}) \tag{5}$$

In general, k, c, h and h^{r} are temperature and spatially dependent, while Q and q are time and spatially dependent.

Let the region Ω be idealized by a system of finite elements and let the unknown temperature T be approximated throughout the solution domain at any time t by

$$T(\underline{x},t) = \sum_{I=1}^{M} N_I(\underline{x})\ T_I(t) = \{N\}^T \{T\} \tag{6}$$

Here the N_I are the interpolation functions defined piecewise element by element and the T_I or $\{T\}$ are the nodal temperatures. The governing equations of the discretized system can be derived by minimizing a functional or by using Galerkin's method [21]. In the Galerkin formulation employed here, the problem is recast in a weighted integral form using the interpolating functions N_I as the weighting functions:

$$\int_{\Omega^e} \{N\}[\nabla \cdot (k\nabla(\{N\}^T \{T\})) + Q - \rho c \frac{\partial}{\partial t} (\{N\}^T \{T\})] \, d\Omega$$

$$- \oint_{\Gamma_2^e} \{N\}[k\nabla(\{N\}^T \{T\}) \cdot \underline{n} + q \tag{7}$$

$$+ h(\{N\}^T \{T\} - T^{ac}) + h^r(\{N\}^T \{T\} - T^{ar})] \, d\Gamma = 0$$

Only a single finite element is considered in the integral (7), as the governing equations of the complete system of elements are obtained by assembling the individual finite element matrices. The surface integral over Γ_2^e refers only to those elements with external boundaries on which condition (3) is given.

Green's first identity is applied to the first volume integral of equation (7) so that the second derivatives do not impose unnecessary continuity conditions between elements. When use is made of the boundary conditions (2) and (3), the integral formulation (7) leads to a set of transient ordinary differential equations for the assemblage of finite elements:

$$[C] \frac{\partial\{T\}}{\partial t} + [K] \{T\} + \{\overline{F}\} + \{\overline{\overline{F}}\} = 0 \tag{8}$$

The components in equation (8) are defined by:

$$[C] = \sum_{e=1}^{E} \int_{\Omega^e} \rho c \{N\} \{N\}^T \, d\Omega \quad , \tag{9}$$

$$[K] = \sum_{e=1}^{E} \int_{\Omega^e} k[B] [B]^T \, d\Omega + \sum_{e=1}^{E} \oint_{\Gamma_2{}^e} (h + h^r) \{N\} \{N\}^T \, d\Gamma \quad ,$$

$$[B] = \nabla\{N\} \quad , \tag{10}$$

$$\{\overline{F}\} = - \sum_{e=1}^{E} \int_{\Omega^e} \{N\} Q d\Omega + \sum_{e=1}^{E} \oint_{\Gamma_2{}^e} \{N\} q d\Gamma \quad , \tag{11}$$

$$\{\overline{\overline{F}}\} = - \sum_{e=1}^{E} \oint_{\Gamma_2{}^e} \{N\} (h^r T^{ar} + h T^{ac}) \, d\Gamma \quad , \tag{12}$$

where the summations are taken over the individual finite element contributions. These integrals are evaluated numerically using Gauss-Legendre quadrature in the applications to be presented later.

The system of nonlinear equations (8) through (12) which defines the discretized problem can be solved using many different types of integration schemes. The implicit one-step Euler backward difference method is employed in this analysis. The time derivative of the temperature is approximated by

$$\frac{\partial\{T\}}{\partial t} = \frac{\{T\}_{(i+1)\Delta t} - \{T\}_{(i)\Delta t}}{\Delta t} \tag{13}$$

where $\{T\}_{(i)\Delta t}$ is assumed known at time $(i)\Delta t$. In the nonlinear analysis, $\{T\}_{(i+1)\Delta t}$ is calculated using a computational scheme that iterates on the out-of-balance heat flow rate for a given time step. At time $(i+1)\Delta t$, the initial approximation of the node point temperatures is calculated by

$$\left(\frac{1}{\Delta t}[C]_{(i)\Delta t} + [K]_{(i)\Delta t}\right)\{T\}^{(0)}_{(i+1)\Delta t} = \frac{1}{\Delta t}[C]_{(i)\Delta t}\{T\}_{(i)\Delta t} - \{\bar{F}\}_{(i+1)\Delta t} - \{\bar{\bar{F}}\}_{(i)\Delta t} \tag{14}$$

As demonstrated in Appendix A, the $(P)^{th}$ correction $\{\Delta T\}^{(P)}$ to the temperature vector $\{T\}_{(i+1)\Delta t}$ is given by

$$[S]^{(P-1)}_{(i+1)\Delta t}\{\Delta T\}^{(P)} = -\left[[S]^{(P-1)}_{(i+1)\Delta t}\{T\}^{(P-1)}_{(i+1)\Delta t} - \frac{1}{\Delta t}[C]^{(P-1)}_{(i+1)\Delta t}\{T\}_{(i)\Delta t} + \{\bar{F}\}_{(i+1)\Delta t} + \{\bar{\bar{F}}\}^{(P-1)}_{(i+1)\Delta t}\right] \tag{15}$$

where

$$[S]^{(P-1)}_{(i+1)\Delta t} = \frac{1}{\Delta t}[C]^{(P-1)}_{(i+1)\Delta t} + [K]^{(P-1)}_{(i+1)\Delta t} \tag{16}$$

is evaluated using temperatures $\{T\}^{(P-1)}_{(i+1)\Delta t}$.

In each iteration, a new temperature vector is computed according to

$$\{T\}^{(P)}_{(i+1)\Delta t} = \{T\}^{(P-1)}_{(i+1)\Delta t} + \{\Delta T\}^{(P)} \tag{17}$$

The iteration continues until convergence is obtained according to the criterion

$$||\{\Delta T\}^{(P)}|| \; / \; ||\{T\}^{(P)}_{(i+1)\Delta t}|| < TOL1 \quad , \tag{18}$$

where TOL1 represents an adjustable tolerance.

The procedure represented by equations (14) through (18) is repeated in each time step of the calculation.

In this application of the finite element method to the inverse problem, the analysis is limited to a one-dimensional model expressed in cylindrical coordinates. The temperatures are assumed to be spatially dependent only upon the radial coordinate r, and an isoparametric [21] discretization is employed,

$$r = \sum_{I=1}^{M} N_I r_I \tag{19}$$

so that r is interpolated using the same functions N_I as those used for T in equation (6). Both linear and quadratic interpolation functions are used in the application to be presented later. These functions are defined for the element natural coordinate system depicted in Figure 3 as follows:

Linear:

$$N_1 = -\frac{1}{2}(\eta - 1) \qquad N_2 = \frac{1}{2}(\eta + 1) \tag{20}$$

Quadratic:

$$N_1 = \frac{1}{2}(\eta^2 - \eta) \quad , \quad N_2 = \frac{1}{2}(\eta^2 + \eta)$$

$$N_3 = 1 - \eta^2 \tag{21}$$

ORNL–DWG 78–10155

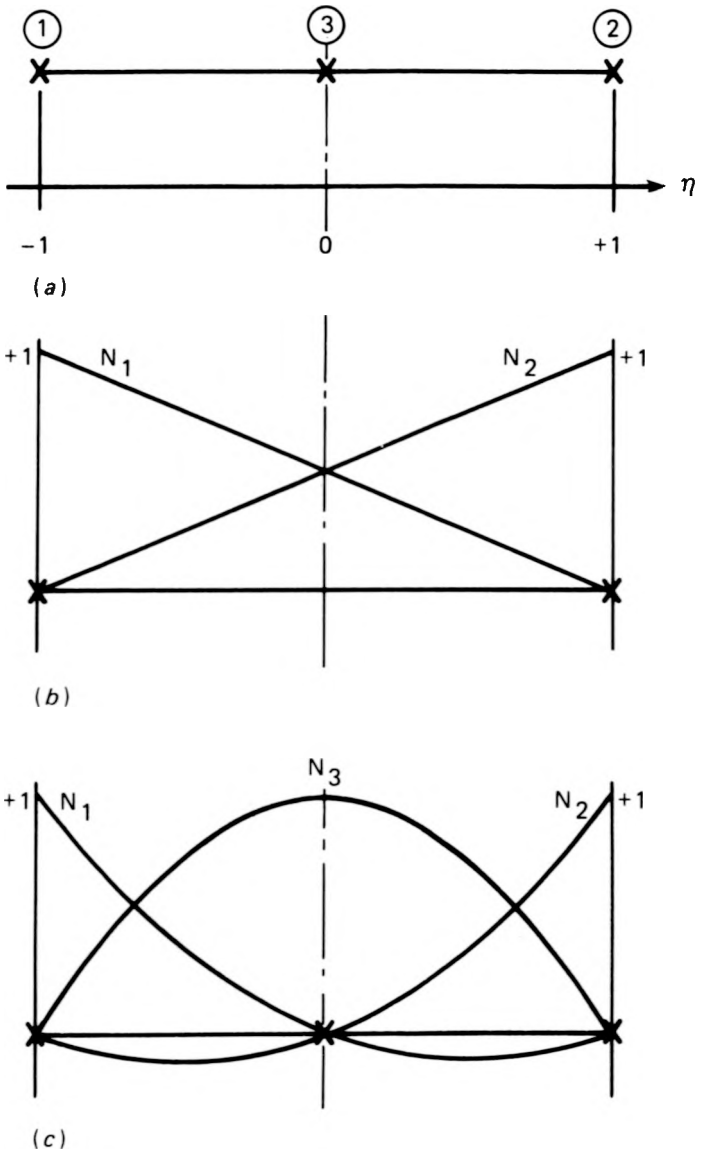

Figure 3. Interpolation functions for one-dimensional element
(a) Element local coordinate system
(b) Linear interpolation
(c) Quadratic interpolation

For the quadratic element, the center node (Figure 3) can be reduced out on the element level using static condensation procedures [28].

VI. FORMULATION OF THE INVERSE PROBLEM

For the purposes of this study, the one-dimensional problem of a cylindrical body with flux boundary conditions at the surface is considered as depicted in Figure 4. The condition

$$T(r^p,t) = T^p(t) \quad \text{at} \quad r = r^p < a \tag{22}$$

is prescribed, while the surface heat flux

$$- k \frac{\partial T}{\partial r} = q(a,t) \quad \text{at} \quad r = a \tag{23}$$

is unknown.

For convenience, a solid cylinder is assumed, but a hollow cylinder with any known boundary condition at the inner surface could be used. The material properties k and c are known functions of temperature T and spatial variable r. The problem is to determine q(a,t) and the spatial temperature distribution $T(r,t)$, $0 \leq r \leq a$, when the temperature history $T(r^p,t) = T^p(t)$ is known at an interior point $r^p < a$.

The method developed by Beck [5], with certain modifications suggested by Muzzy, et al [20], is used in the solution of the nonlinear inverse problem presented here. Beck's technique focuses on the observation that the temperature response at an interior location is delayed and damped with respect to changes at the surface of the body, as verified by Burggraf's exact linear solution [9]. To effectively deal with this observation, Beck determines the surface heat flux q(a,t) at time t using interior temperatures T^p measured at times greater than t. A common difficulty with other numerical inverse procedures (Reference [6], for example) is the occurrence of violent oscillations or instabilities in

ORNL–DWG 78–10156

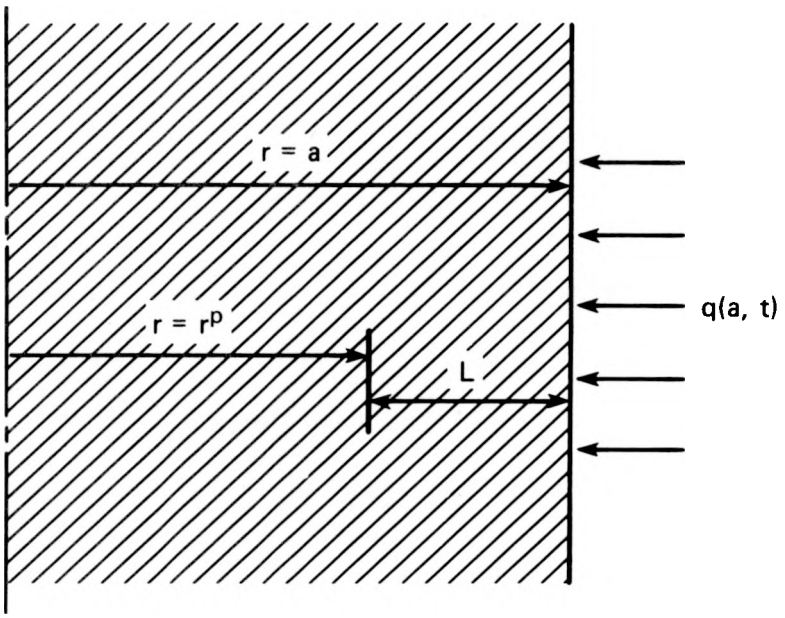

Figure 4. Geometry of heated cylindrical rod

the calculated heat flux when the time steps are reduced to sufficiently small values. Beck's approach permits the use of small time steps for improved accuracy in the heat flux calculations without encountering these instabilities. His method also tends to reduce oscillations in the computed surface flux due to experimental errors incurred in measurement of the interior temperatures T^p.

In the application of Beck's method, the surface heat flux is represented by a vector of elements $(q_0, q_1, \ldots, q_n)$ such that in a given time step Δt, $q(a,t)$ is represented by

$$q(a,t) = q_{(i)\Delta t} \quad (i-1)\Delta t < t \leq (i)\Delta t \quad , \quad i \geq 1 \tag{24}$$

For a given $i \geq 1$, it is assumed that $q_{1\Delta t}, q_{2\Delta t}, \ldots, q_{(i)\Delta t}$ are known. To determine $q_{(i+1)\Delta t}$, an analysis interval consisting of $J \geq 1$ time steps is selected, as depicted in Figure 5. In the next step of the calculation, q is estimated over the analysis interval $(i)\Delta t < t \leq (i+J)\Delta t$ using relations that take the trend of q into account.[1] For the first time step in the analysis interval,

$$q_{(i+1)\Delta t} = q_{(i)\Delta t} + (q_{(i)\Delta t} - q_{(i-1)\Delta t}) \tag{25}$$

and for the "future" time steps

$$q_{(i+j)\Delta t} = q_{(i+j-1)\Delta t} + \beta(q_{(i+j-1)\Delta t} - q_{(i+j-2)\Delta t}) \tag{26}$$

[1] In his paper, Beck examines both constant and linearly varying heat flux estimates over the analysis interval.

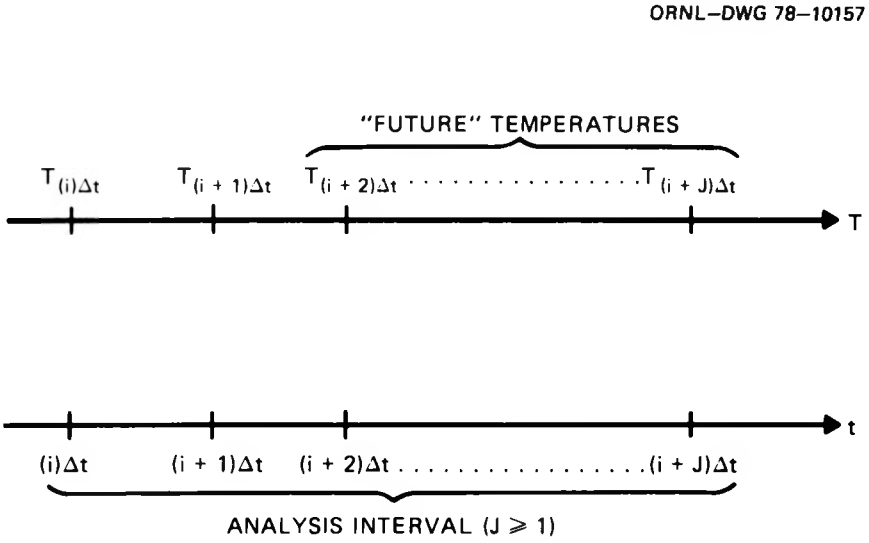

Figure 5. Analysis interval for computing surface heat flux $q_{(i+1)\Delta t}$

for $2 \leq j \leq J$, where $0 \leq \beta \leq 1$ is an adjustable parameter.[2] Then the boundary value problem (equations (1) through (5)), cast in the discretized finite element formulation (equations (8) through (12)), is solved over the analysis interval $(i)\Delta t < t \leq (i+J)\Delta t$, using conditions (25) and (26).

The objective of the method is to select $q_{(i+1)\Delta t}$ to achieve the closest agreement in a least squares sense between the computed and input temperatures at r^p over the analysis interval. This is accomplished by minimizing the weighted sum of squares function

$$f(q) = \sum_{j=1}^{J} w_j (T_{(i+j)\Delta t} - T^p_{(i+j)\Delta t})^2 \tag{27}$$

with respect to the parameter $q_{(i+1)\Delta t}$. In equation (27), the weights are defined by $w_j = j^2$ and $T_{(i+j)\Delta t}$, $T^p_{(i+j)\Delta t}$ are the computed and input temperatures at the interior point r^p. The minimization is done using an iterative procedure that involves direct sampling of the function (27) and adjustment of $q_{(i+1)\Delta t}$ in each iteration.[3]

The solution value of $q_{(i+1)\Delta t}$ is taken as the accepted value of $q(a,t)$ over the single time step Δt only. The analysis interval is shifted by one time step and the process is repeated. For the special case $J = 1$, no future temperatures are used and least squares minimization is not required.

---

[2] q_0 is determined from conditions at the initial time.

[3] In his formulation, Beck uses an analytical scheme to minimize the summed square function f.

For convective boundary conditions, a heat transfer coefficient can be computed in each time step from the expression

$$h_{(i)\Delta t} = \frac{q_{(i)\Delta t}}{(T^{w}_{(i)\Delta t} - T^{ac}_{(i)\Delta t})} \tag{28}$$

As an alternate formulation, the iteration scheme outlined above can be performed on the heat transfer coefficient $h_{(i)\Delta t}$ and the surface heat flux then computed from

$$q_{(i)\Delta t} = h_{(i)\Delta t}(T^{w}_{(i)\Delta t} - T^{ac}_{(i)\Delta t}) \tag{29}$$

The latter scheme is employed by Muzzy, et al [17] in a finite difference application of Beck's method.

Some of the modifications to Beck's method suggested in Reference [17] have been implemented in the procedure presented here. First of all, a weighted least squares criterion is used in the function (27). The weights reflect that the temperature difference at time $(i+j)\Delta t$ has more influence on $q_{(i+1)\Delta t}$ for increasing j over the analysis interval consisting of an appropriate number of time steps. Beck's formulation is obtained by defining $w_j \equiv 1$ for all j.

Secondly, before minimization of the summed square function (27) proceeds for a given analysis interval, $q_{(i+1)\Delta t}$ is adjusted iteratively to satisfy the requirement

$$|T_{av} - T^{p}_{av}| < TOL2 \tag{30}$$

for some prescribed TOL2 > 0, where T_{av} is given by

$$T_{av} = \frac{1}{W} \sum_{j=1}^{J} w_j \, T_{(i+j)\Delta t} \quad , \quad W = \sum_{j=1}^{J} w_j \tag{31}$$

and T^p_{av} is similarly defined. The resultant estimate for $q_{(i+1)\Delta t}$ is then refined in the minimization procedure for the function (27). This ensures that the input and computed temperatures at r^p agree closely in an averaged sense before minimization of the summed square function (27) is carried out. Otherwise, it may be possible for the algorithm to calculate $q_{(i+1)\Delta t}$ from a relative minimum rather than from the true minimum of the function (27) on the analysis interval. This problem is discussed in more detail in Reference [20].

A crucial factor in Beck's formulation is the relationship between the magnitude of the time step Δt and the required number of time steps J in the analysis interval, given a temperature probe located a distance L from the heated surface. Beck [5] explores this relationship by studying sensitivity coefficients that define the temperature change at an interior point due to a unit step in surface heat flux. He examines a one-dimensional model with the temperature probe fixed at distance $\frac{L}{a} = 1$ from the surface. Using the criteria derived from the sensitivity coefficients for this model, Beck recommends values of J that are appropriate for given values of the dimensionless time step $\Delta\tau = \frac{\alpha\Delta t}{a^2}$. The value of J is increased as the magnitude of $\Delta\tau$ is reduced, roughly preserving the length $J \cdot \Delta\tau$ of the analysis interval. Muzzy, et al [20] also study this relationship in applying Beck's formulation. Some additional results are presented in the numerical applications in this report. For a detailed discussion of this topic, the reader is referred to Beck's paper.

VII. NUMERICAL APPLICATIONS

The inverse formulation developed in the preceding sections has been implemented in the digital computer program INCAP, as described in Appendices B and C of this report. The primary objective of this study is to compare the inverse calculations of program INCAP with those of program ORINC using representative temperature transients recorded by thermocouple sensors in the heater rod bundle. Prior to making these comparisons, the performance of program INCAP in solving the inverse problem is evaluated in two test problems.

A heater rod cross section[4] and the corresponding one-dimensional finite element discretization used in the inverse analysis are depicted in Figures 6 and 7. The electric heater rods are from 548.64 to 640.08 cm (18 to 21 ft) in length, 1.077 cm (0.424 in.) in diameter, and have dual-sheath design. The outer sheath is 0.025 cm thick (0.010 in.) stainless steel; the inner sheath is 0.076 cm thick (0.030 in.) stainless steel and is grooved to accept the 0.051 cm (0.020 in.) chromel vs. alumel thermocouples. The next inner layer is boron nitride (BN), which electrically insulates the heating element from the stainless steel sheaths. In the section of the rod from which the cross section of Figure 6 is extracted, the heater element consists of an Inconel 600 tube.[5] The core of the heater element is filled with magnesium oxide (MgO), which is both a filler and insulator between the heating element and the central rod thermocouple sheaths.

---

[4]The heater rod cross section selected for the test models is that one identified in Reference [4] for LEVEL G (ZONE I).

[5]As described in Reference [4], the heater element configuration and heater output vary over the length of the rod.

ORNL–DWG 78–10158

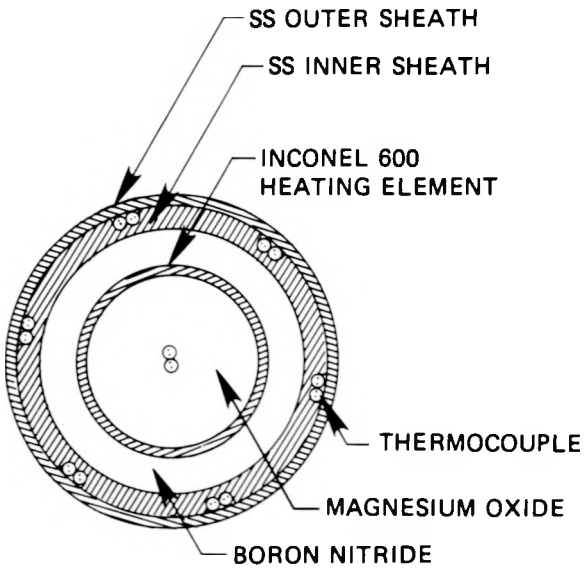

(a)

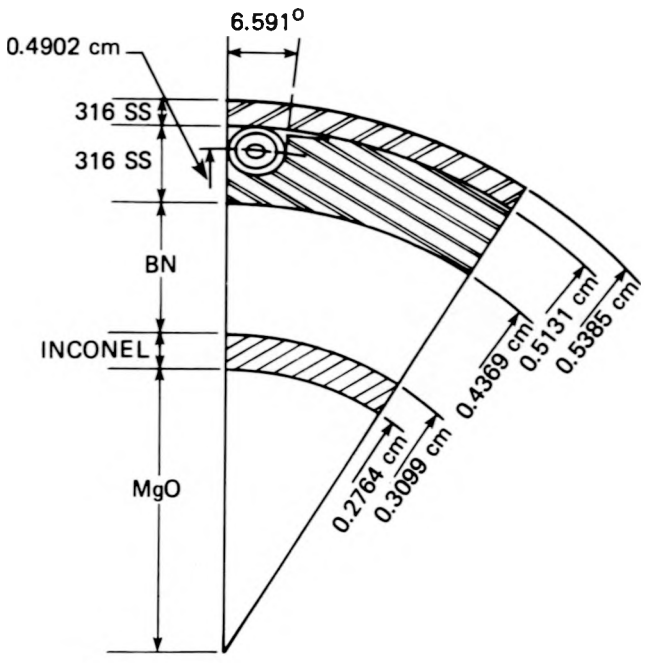

(b)

Figure 6. Electrically-heated rod containing thermocouple sensors
(a) Cross section
(b) Dimensions

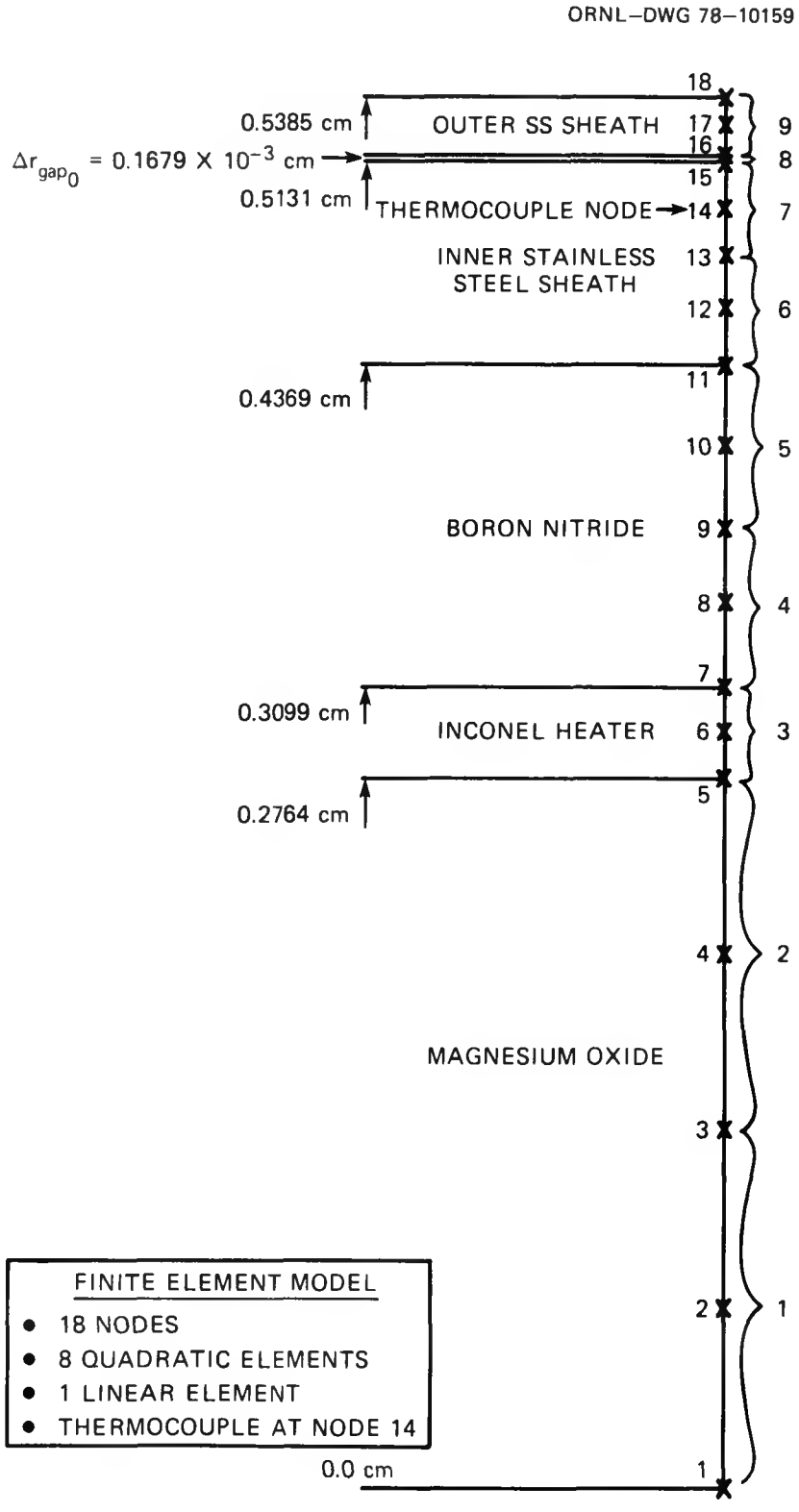

Figure 7. One-dimensional finite element model of heater rod cross section

The transient response of the heater rod is modeled as a coupled heat conduction and mechanical deformation problem due to the presence of a small air gap between the stainless steel sheaths that varies in width with temperature. The fabrication process that reduces the heater rod to its final diameter often creates an imperfect fit between the inner and outer sheaths at the thermocouple locations and produces a gap between the thermocouple junction and the outer sheath. The thermocouple is welded to the inner sheath, causing the gap between the junction and outer sheath to grow with increasing fluid temperature and to close with increasing heater power. Correspondingly, the change in the gap width alters the temperature profile in the cross section.

A one-dimensional model developed in Reference [4] is used to model the mechanical response of the gap:

$$\Delta r_{gap} = \Delta r_{gap_0} + r_{16}(\mathrm{EXP}[C_1(T_{16} - T_{16_0}) + \frac{C_2}{2}(T_{16}^2 - T_{16_0}^2) + \frac{C_3}{3}(T_{16}^3 - T_{16_0}^3)] - 1) - r_{15}(\mathrm{EXP}[C_1(T_{15} - T_{15_0}) + \frac{C_2}{2}(T_{15}^2 - T_{15_0}^2) + \frac{C_3}{3}(T_{15}^3 - T_{15_0}^3)] - 1) \quad (32)$$

In equation (32), the quantities Δr_{gap_0}, T_{16_0}, T_{15_0} are the steady-state gap width and steady-state nodal temperatures determined in an initial steady-state configuration. The expansion coefficients C_i(i=1,3) are

determined in situ as part of a rod calibration procedure [29] for each test. In calculating the thermomechanical response of the heater rod model, the gap width Δr_{gap} and the appropriate geometric variables of the finite element model (equations (8) through (12)) are adjusted in each iteration of the solution process described in equations (14) through (18).

The thermophysical properties of thermal conductivity k and specific heat c are dependent upon temperature and the spatial coordinate. Except for the thermal conductivities of MgO and BN, these properties are determined for each material as a function of temperature from an optimum polynomial fit to available data, as given in Reference [4]. The thermal diffusivity for the MgO and the thermal conductivity for the BN are determined in situ as part of the rod calibration procedure [29] prior to each test.

The first numerical example[6] was selected to evaluate the performance of the technique in solving the inverse problem for the finite element model of Figure 7. The periodic surface heat flux depicted in Figure 8 was used as boundary condition input for a direct solution. This boundary condition is included because the ramp in heat flux is typical of surface transients in the test loop and because the finite element formulation used by Hore, et al [27] demonstrated divergence in the surface heat flux for a similar periodic problem. The temperature transient of Figure 8 was

---

[6]The finite element inverse calculations described in this section were performed using TOL1=.001, equation (18); TOL2=1.0, equation (30); β=0.5, equation (26); Δt=0.05 seconds, which is equal to the data acquisition interval for the thermocouple sensors in the heater rod. For each analysis, the iterative procedure for minimizing the summed square function (equation (27)) was terminated when the uncertainty in the value of $q_{(i+1)\Delta t}$ was less than 1%.

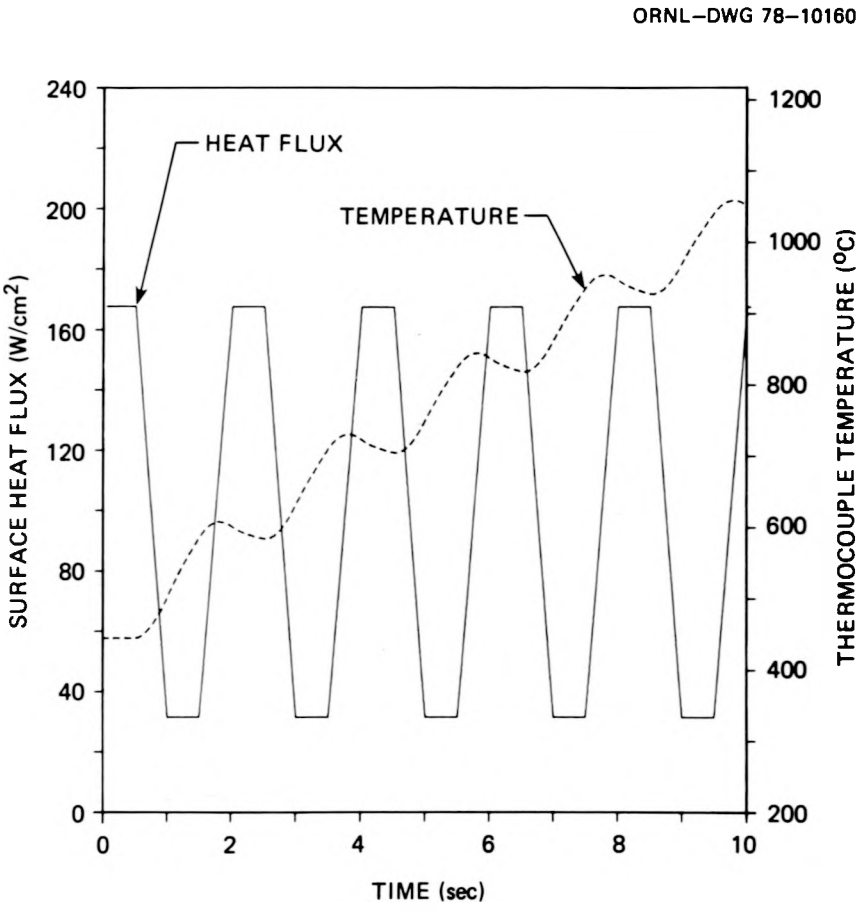

Figure 8. First test case: Imposed surface heat flux and calculated thermocouple temperature of direct solution

calculated at the thermocouple node 14 of the discrete model using a heat generation rate fixed at $Q = 9.19 \times 10^3$ watts/cm^3. With the temperature transient of Figure 8 serving as input, the corresponding inverse analysis was performed in an attempt to recreate the periodic surface heat flux boundary condition. Computed results were obtained using no "future" temperatures, one, and two "future" temperatures (corresponding to J = 1, 2, and 3) in the inverse solution. In Figures 9 through 11, the surface heat flux calculated for each J value is compared with the input boundary condition of the direct problem. The calculated and input thermocouple temperatures at node 14 are also compared for each case in these figures; however, the error in temperatures (TOL2 = 1.0) is not discernible on the scale of these plots. All three inverse solutions follow the input surface flux of the direct problem.

In the second test problem, the procedure used in the first problem is repeated to evaluate the capabilities of INCAP to track severe transients of varying time lengths ($2\Delta t$, $4\Delta t$, $6\Delta t$, $8\Delta t$, $10\Delta t$, $\Delta t = 0.05$ secs), as depicted in Figure 12. The inverse problem again is computed using no "future" temperatures, one and two "future" temperatures and the results are illustrated in Figures 13 through 15. Results obtained from this and the first test problem demonstrate that the solutions using "future" temperatures reduce oscillations in the computed surface heat flux, but tend to "round off" rapid changes as J is increased. For the finite element model of Figure 7 and a selected time step of $\Delta t = .05$ seconds, the use of one "future" temperature appears optimal for reducing oscillations.

Turning now to the primary objective of this study, inverse calculations from programs INCAP and ORINC are compared for two actual thermocouple

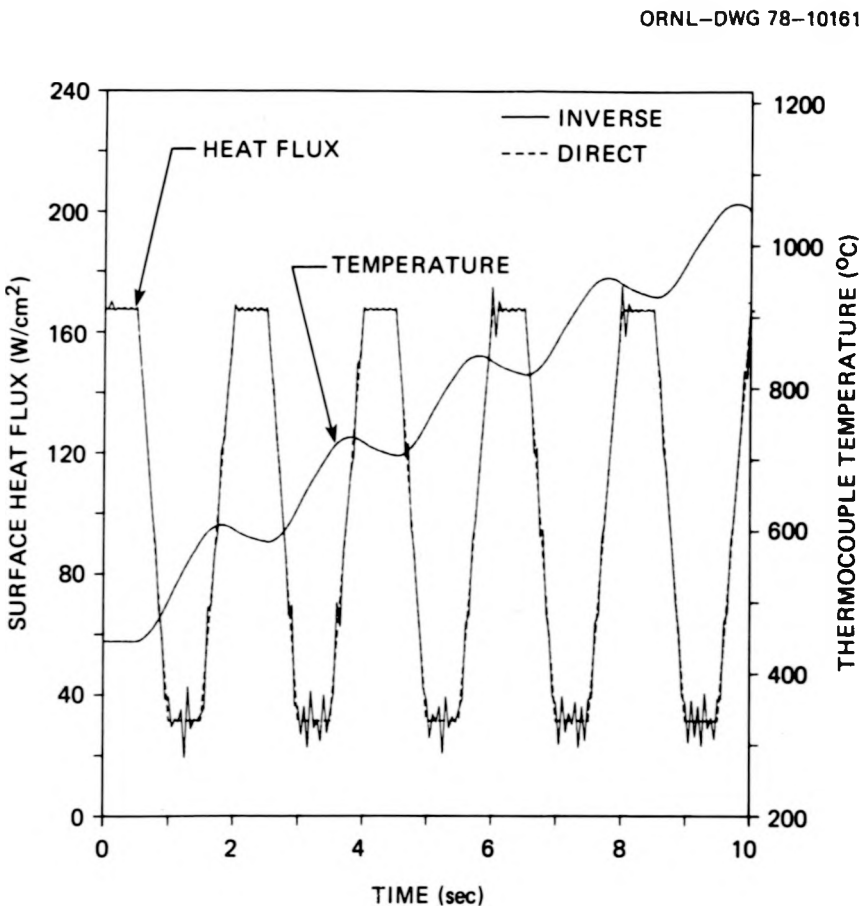

Figure 9. First test case: Comparison of direct solution with inverse solution using no future temperatures (J = 1)

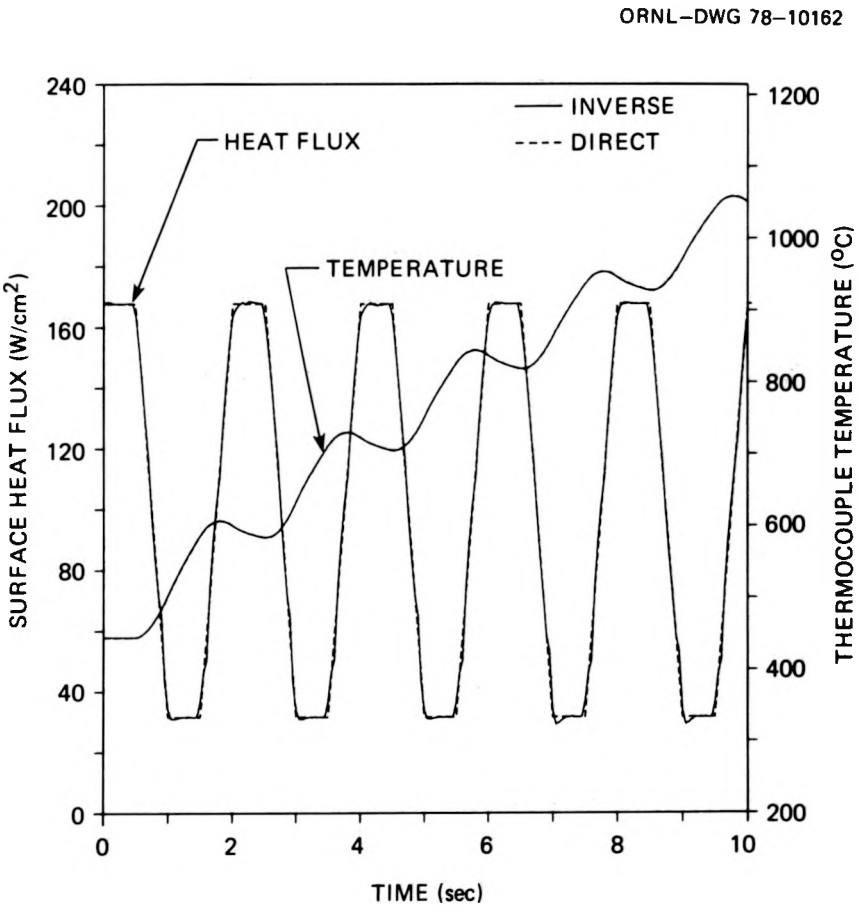

Figure 10. First test case: Comparison of direct solution with inverse solution using one future temperature (J = 2)

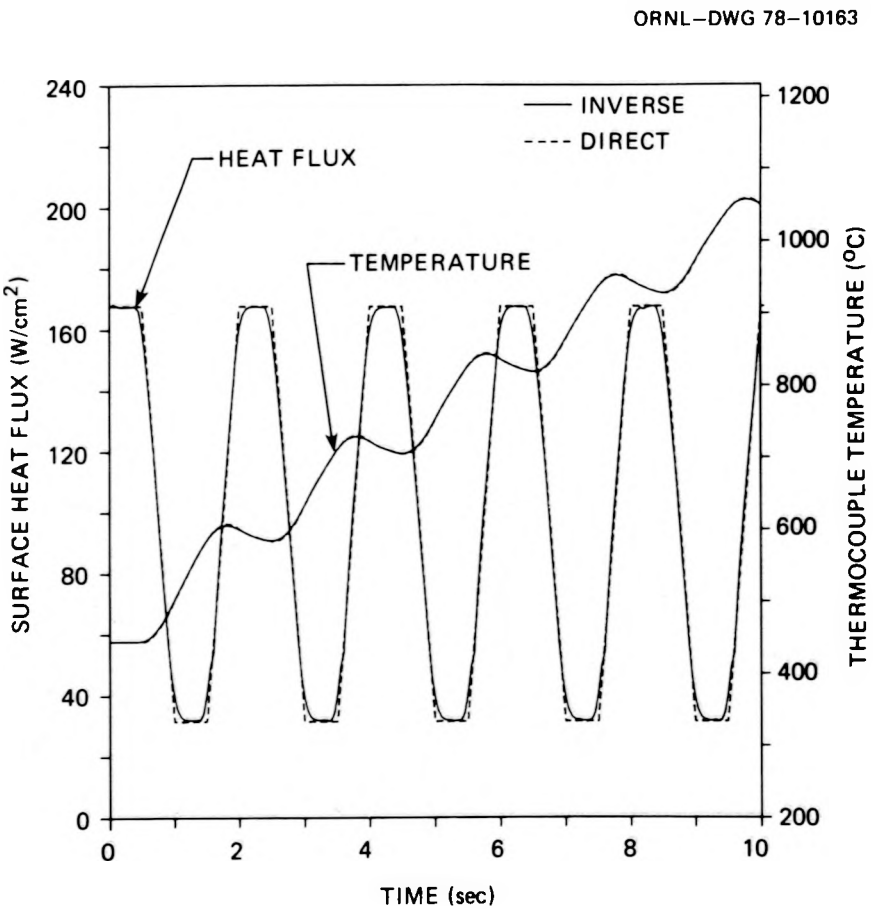

Figure 11. First test case: Comparison of direct solution with inverse solution using two future temperatures (J = 3)

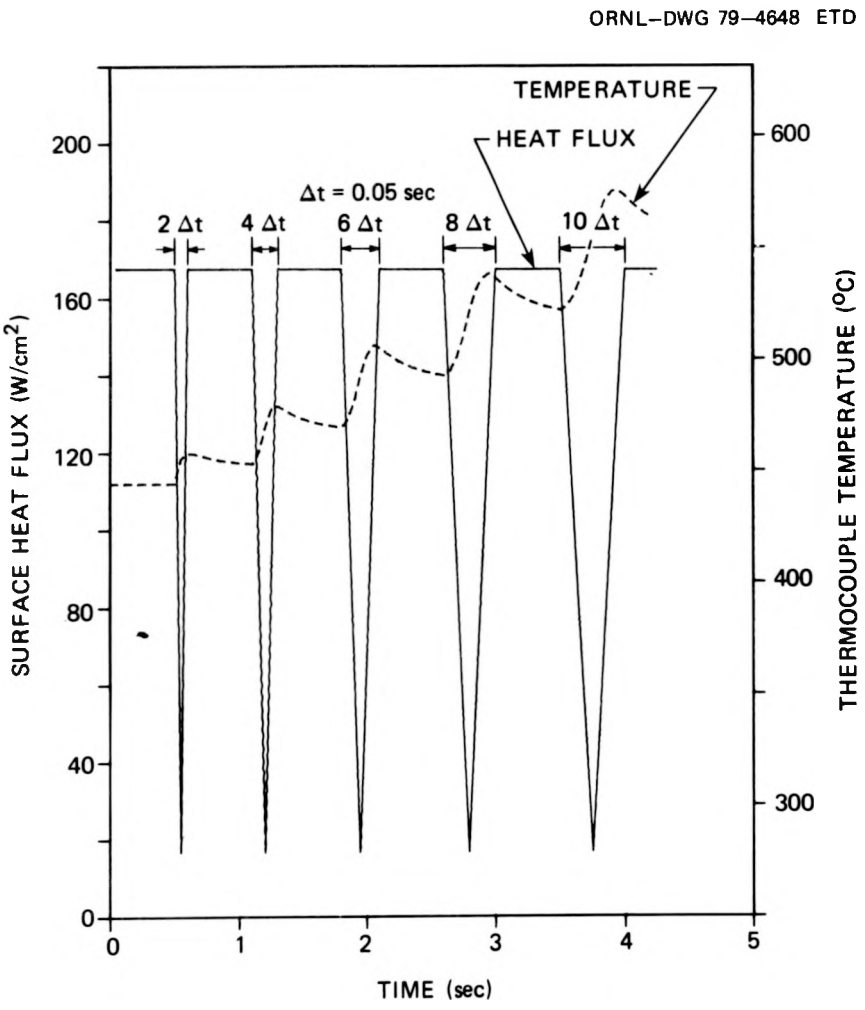

Figure 12. Second test case: Imposed surface heat flux and calculated thermocouple temperature of direct solution

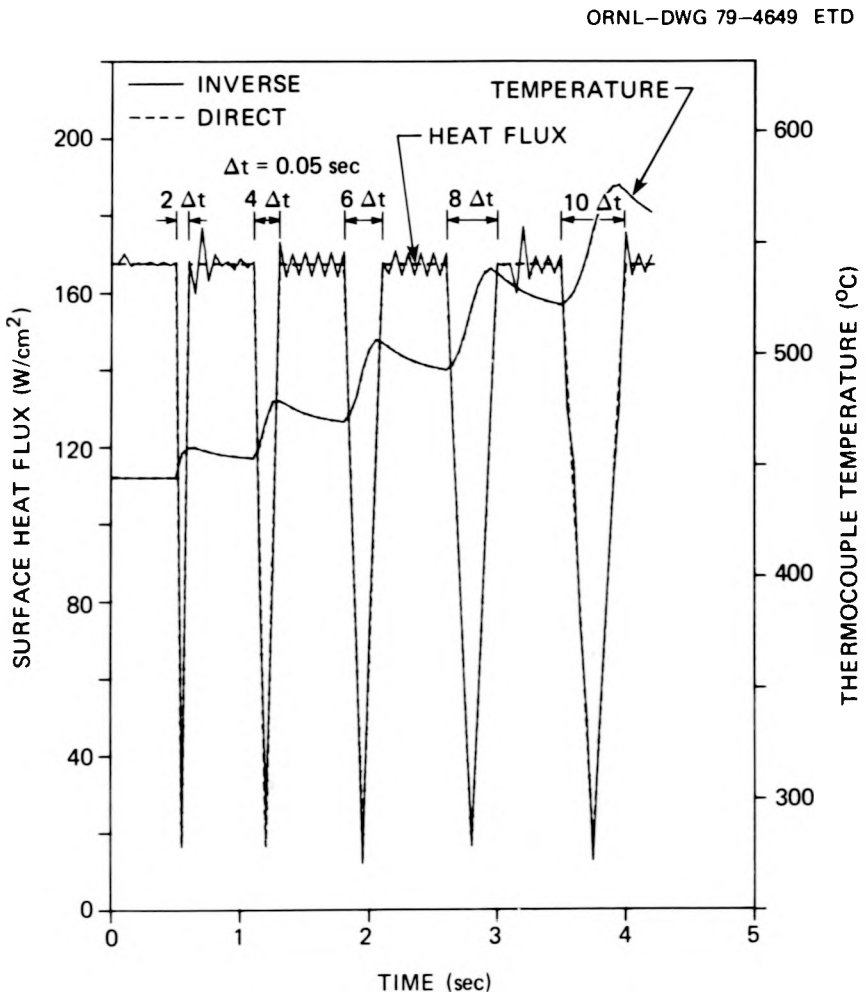

Figure 13. Second test case: Comparison of direct solution with inverse solution using no future temperatures (J = 1)

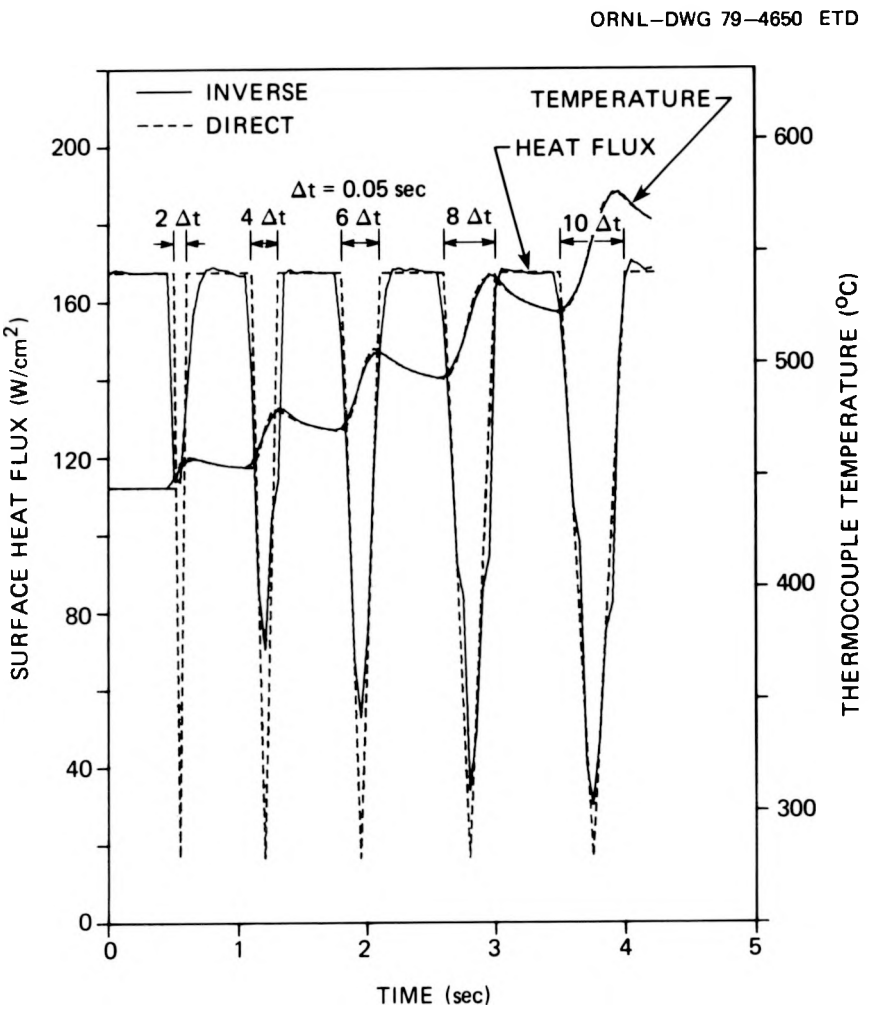

Figure 14. Second test case: Comparison of direct solution with inverse solution using one future temperature (J = 2)

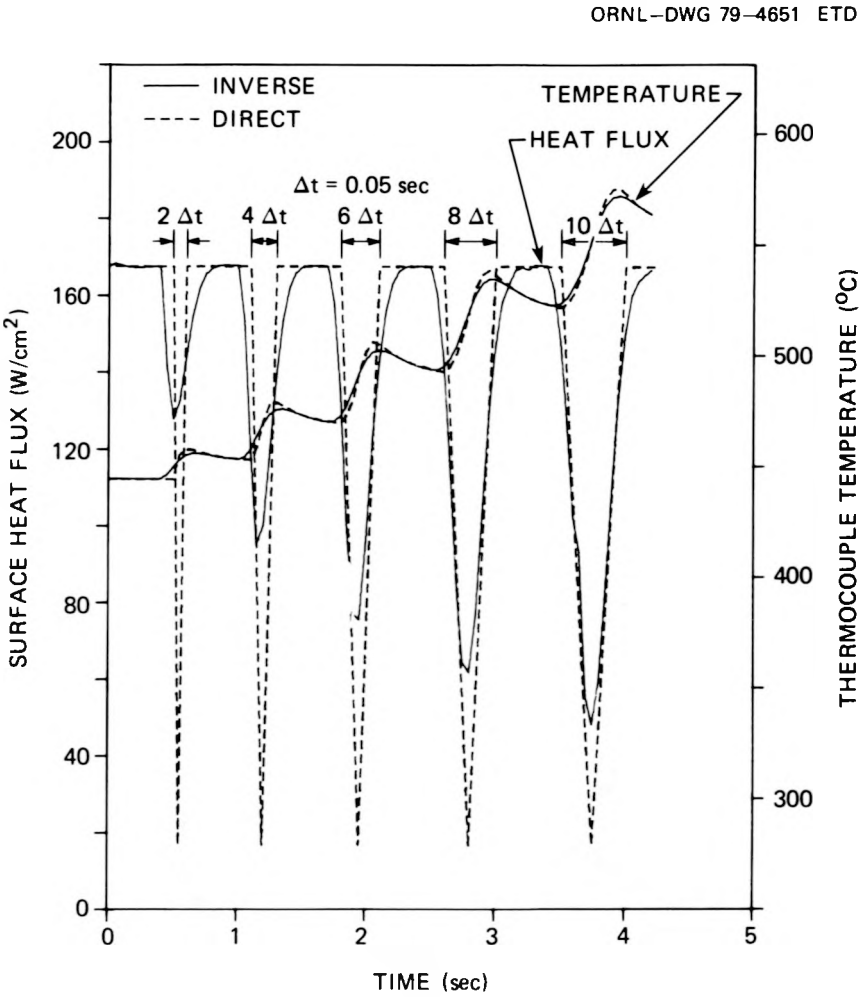

Figure 15. Second test case: Comparison of direct solution with inverse solution using two future temperatures (J = 3)

transients recorded during a representative BDHT blowdown test. For the comparison, blowdown test 105 [30] was selected and two examples, at thermocouples[7] TE-325BG and TE-325AD of rod bundle 1, were run on both programs. The heater power input at the appropriate level of the rod and the measured thermocouple temperatures of the transient are depicted in Figure 16 for TE-325BG and in Figure 20 for TE-325AD. The results of the inverse analyses for thermocouple TE-325BG are plotted in Figures 17 through 19 and those for TE-325AD in Figures 21 through 23 for the first 10 seconds of the test, the significant period of the transient. Included are plots of surface heat flux and surface temperatures computed by programs INCAP and ORINC. Results from INCAP include solutions utilizing no "future" temperatures, one, and two "future" temperatures; ORINC is capable of using contemporary temperatures only. Figures 16 and 20 also compare the thermocouple temperatures of the INCAP inverse solution for J = 2 with the measured thermocouple temperatures; as in the first test case, the error in temperatures is not discernible on the scale of these plots.

Comparisons of the inverse calculations (Figures 17 through 19 and 21 through 23) performed by INCAP and ORINC for the two thermocouple transients indicate good agreement between the finite element and the finite difference inverse techniques for the rod configuration of Figure 6. Results from the test problems (Figures 8 through 15)

[7] The heater rod finite element model depicted in Figure 7 was used in the inverse analysis of TE-325BG. The same configuration was used for TE-325AD, except for small changes in position of some material interfaces and in the bias gap width. The position of these thermocouples in THTF bundle 1 and a complete description of rod geometry are given in Reference [4].

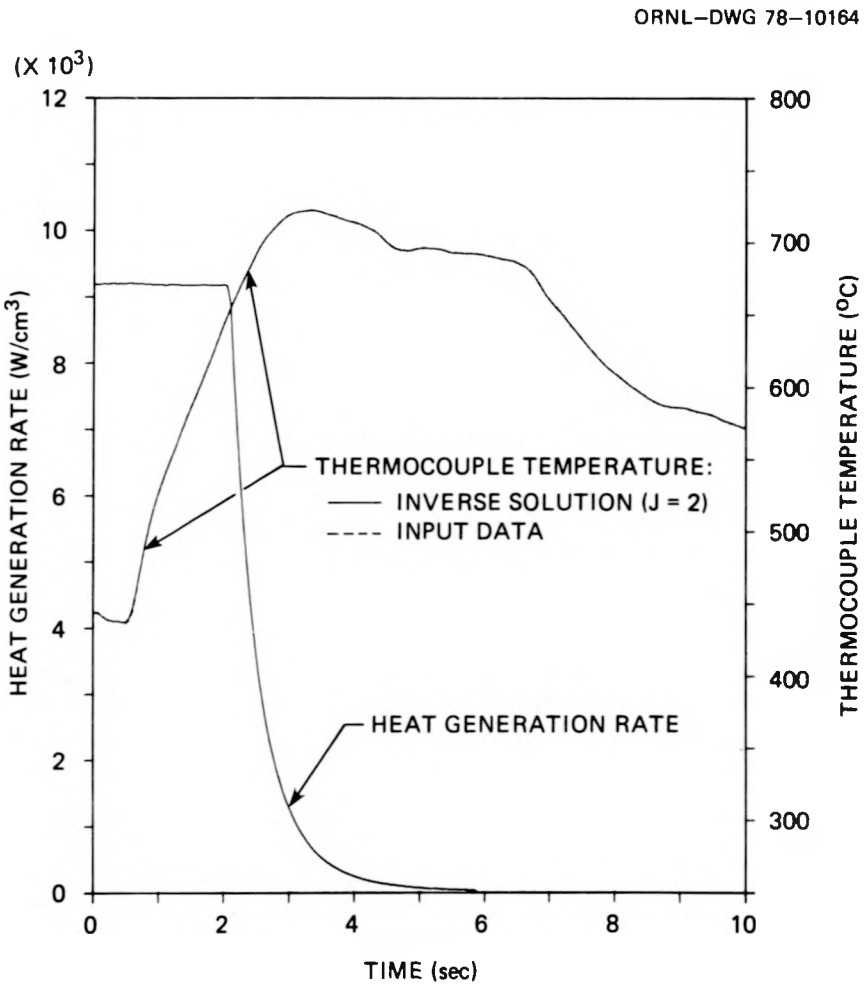

Figure 16. THTF test 105, thermocouple TE-325BG, bundle 1: Heater power input at level G (Zone I) and thermocouple transient for first 10 seconds of test

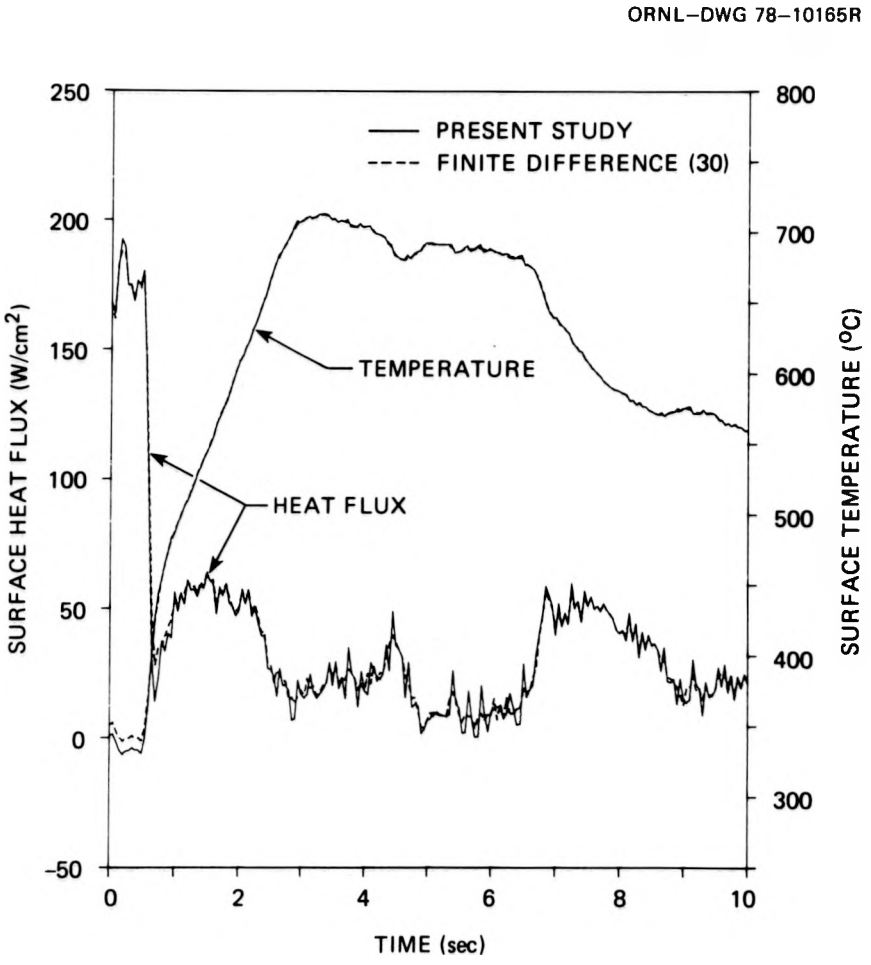

Figure 17. Thermocouple TE-325BG: Comparison of INCAP inverse solution using no future temperatures (J = 1) with ORINC solution

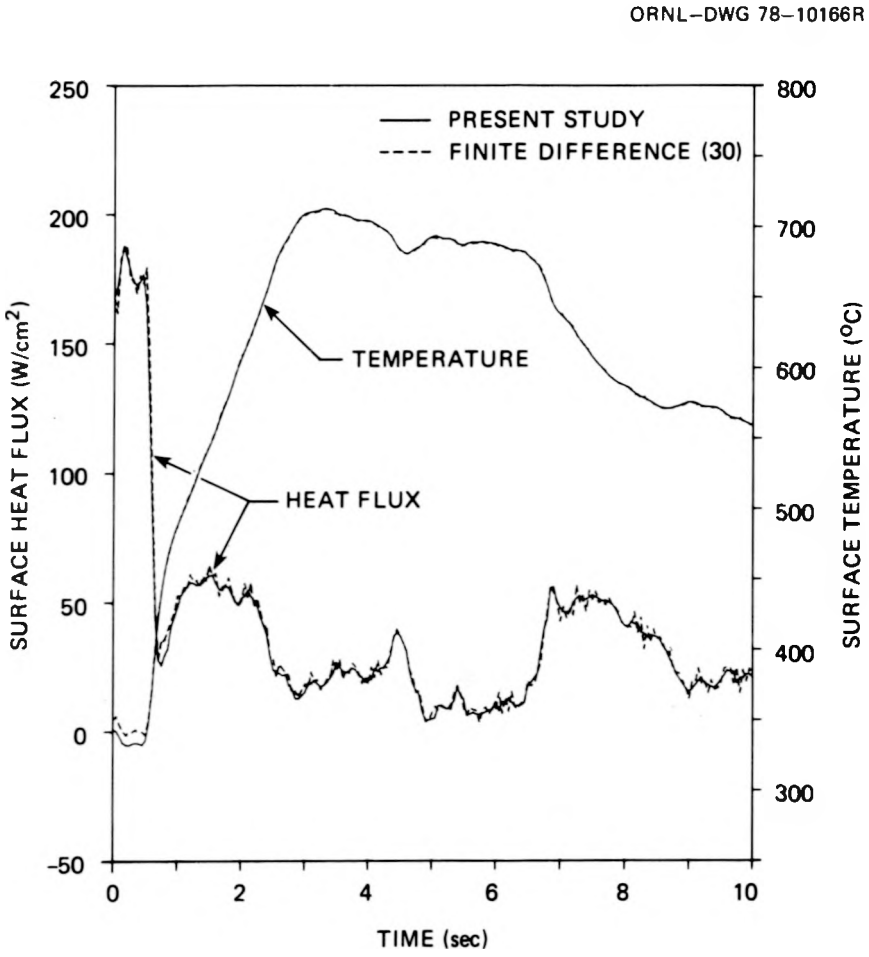

Figure 18. Thermocouple TE-325BG: Comparison of INCAP inverse solution using one future temperature (J = 2) with ORINC solution

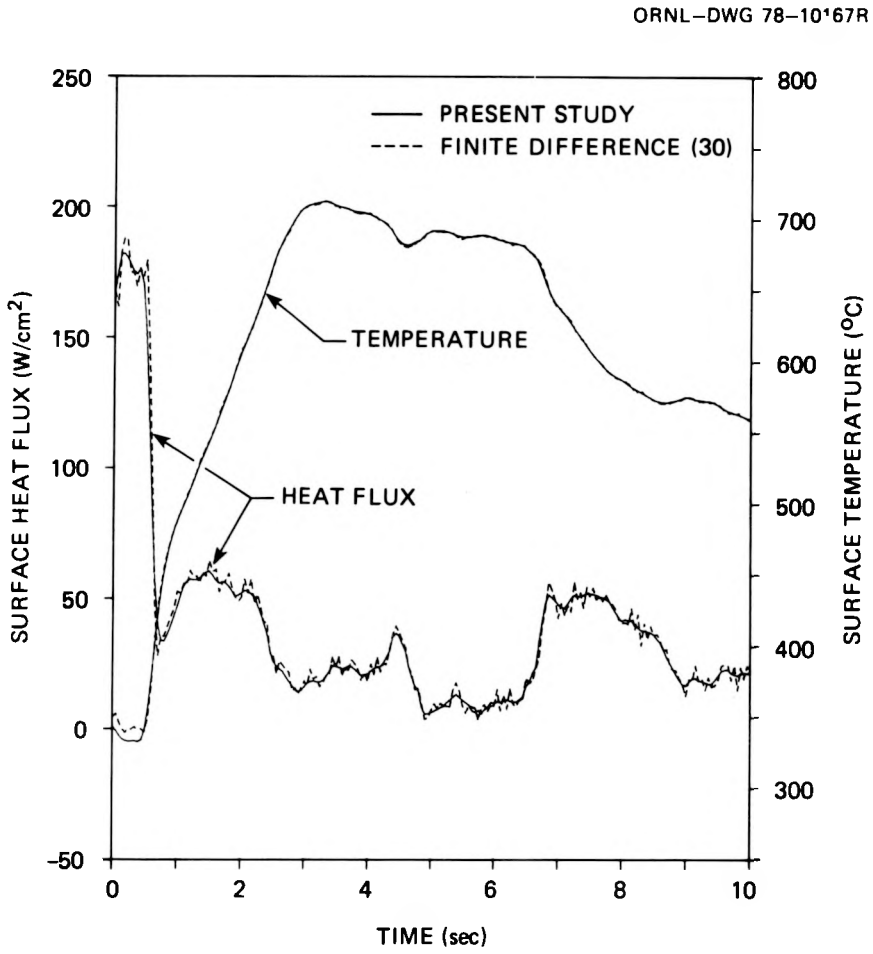

Figure 19. Thermocouple TE-325BG: Comparison of INCAP inverse solution using two future temperatures (J = 3) with ORINC solution

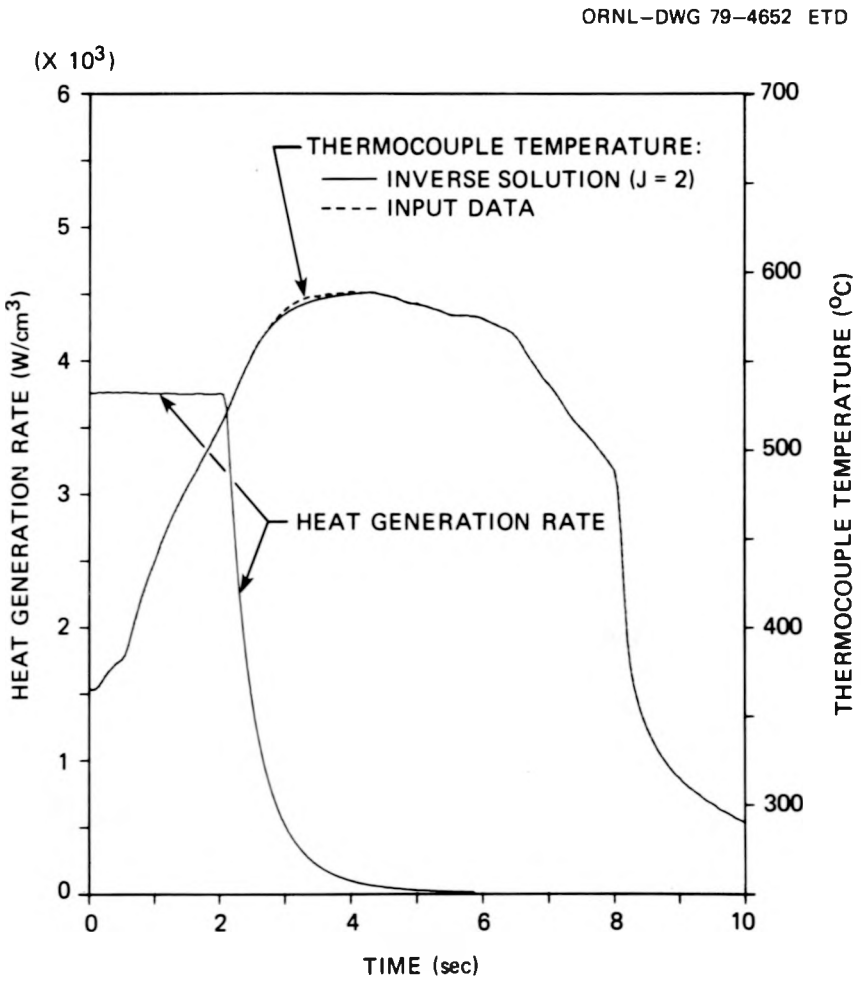

Figure 20. THTF test 105, thermocouple TE-325AD, bundle 1: Heater power input at level D (Zone III) and thermocouple transient for first 10 seconds of test

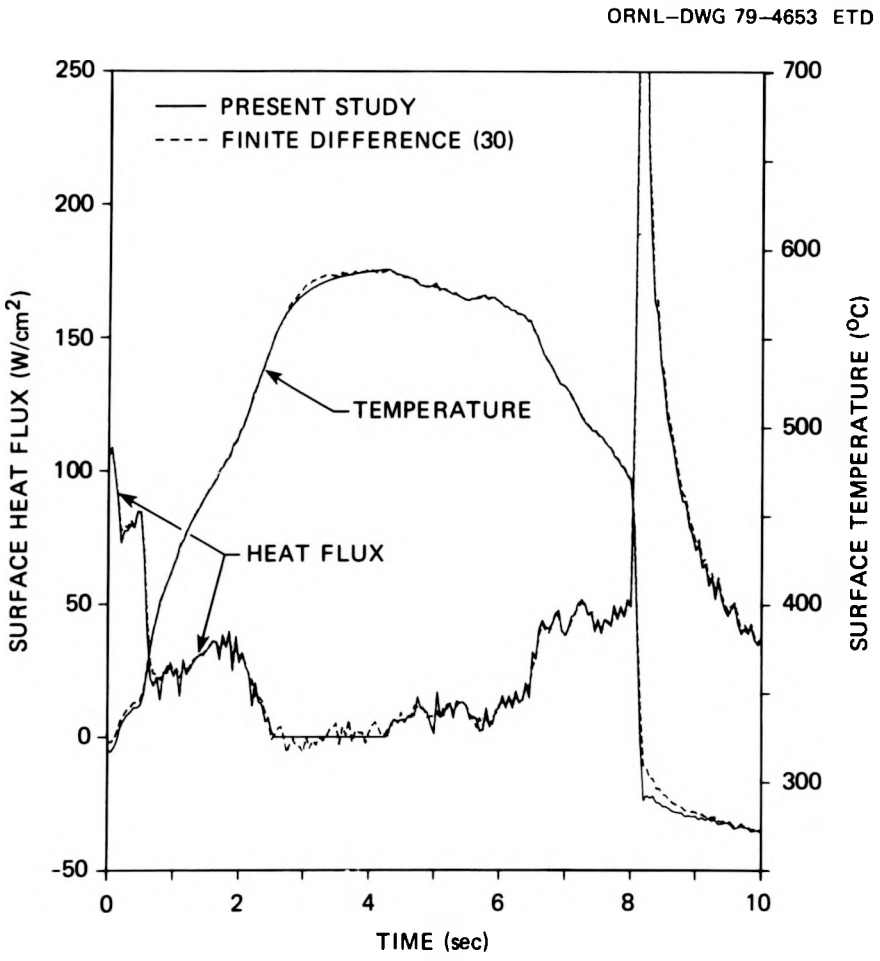

Figure 21. Thermocouple TE-325AD: Comparison of INCAP inverse solution using no future temperatures (J = 1) with ORINC solution

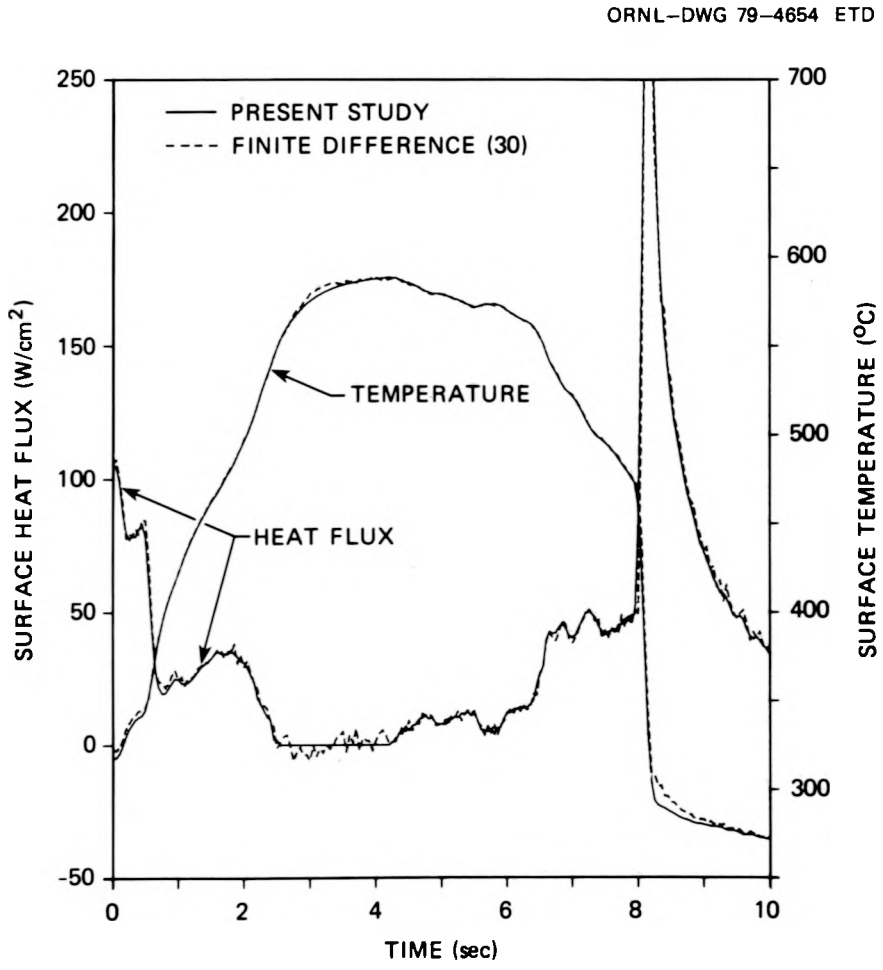

Figure 22. Thermocouple TE-325AD: Comparison of INCAP inverse solution using one future temperature (J = 2) with ORINC solution

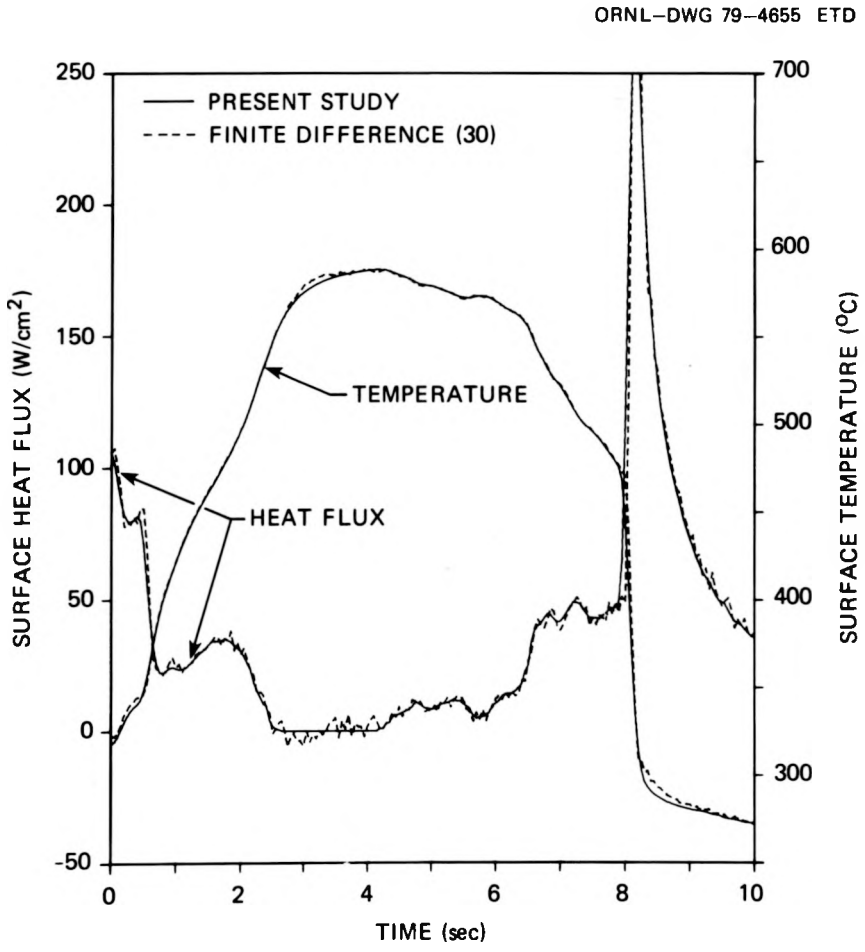

Figure 23. Thermocouple TE-325AD: Comparison of INCAP inverse solution using two future temperatures (J = 3) with ORINC solution

suggest that the use of one future temperature in the INCAP analyses is adequate to remove some of the "roughness" from the computed results without severe rounding of rapid changes in surface heat flux.

The table below gives comparisons of the CPU times required for execution of the BDHT inverse calculations on the IBM 360/195 computer using programs INCAP and ORINC. The relatively large CPU times used in

Comparison of CPU Time Required on the IBM 360/195
For Inverse Analyses of Measured Transients
Using INCAP and ORINC

	Future Temperatures	TE-325BG	TE-325AD
INCAP	0	17 secs	19 secs
	1	94 secs	112 secs
	2	133 secs	180 secs
ORINC	0	3.6 secs	3.6 secs

the INCAP analyses are due to the substantial number of iterative solutions demanded by Beck's inverse technique. In the comparisons presented here, program INCAP is computationally less efficient than ORINC; however, it should be emphasized that Beck's method is applicable to a larger class of problems than the algorithm used in ORINC. Beck [5] has demonstrated that, for the temperature probe located away from the heated surface such that L/a=1, and for sufficiently small dimensionless time steps $\Delta\tau=\alpha\Delta t/a^2$, inclusion of "future" temperatures in the inverse analysis is required to prevent violent oscillations or instabilities in the heat flux

calculations. The algorithm employed in ORINC is not applicable to those problems requiring "future" temperatures.

VIII. SUMMARY AND CONCLUDING REMARKS

In this paper, a formulation of the nonlinear inverse heat conduction problem has been presented that is applicable to composite bodies with temperature-dependent thermophysical properties. This formulation, based on a finite element model of the direct problem and on Beck's nonlinear estimation procedure, was implemented in the digital computer program INCAP. Applications of the finite element inverse program INCAP to an electrically-heated composite rod were examined in this study. In two test examples, a known heat flux was imposed on the surface of the rod. The inverse calculations from INCAP followed the input surface heat flux in each of the direct problems, with the use of one "future" temperature optimal for reducing oscillations without severe "rounding" of rapid changes in the computed flux. Finally, program INCAP was used in a comparative study with the finite difference inverse code ORINC. Comparisons were made between INCAP and ORINC for two actual thermocouple transients recorded at interior thermocouple sensors in the heater rods during a simulated loss-of-coolant accident. The surface heat flux and surface temperatures computed by programs INCAP and ORINC were found to be in good agreement for both of the thermocouple transients. Program INCAP is computationally less efficient than ORINC when applied to the geometry of the electrically-heated rods of bundle 1; for INCAP solutions using no "future" temperatures (J=1), the average ratio of INCAP-to-ORINC CPU time on the IBM 360/195 computer is approximately 5-to-1. However, the algorithm used in INCAP is applicable to a much larger class of inverse problems than that used in ORINC.

The results presented here clearly demonstrate that the inverse formulation based on the finite element technique and Beck's second method is capable of successfully treating experimental data. Consideration of "future" temperatures in calculating surface heat flux permits the use of small dimensionless time steps while avoiding severe oscillations or numerical instabilities in the computed results. This technique also reduces oscillations in the calculated heat flux that are due to experimental errors incurred in temperature measurements.

Studies are under way to extend the formulation presented here to treat the coupled inverse heat conduction-thermal deformation problem in two and three dimensions. While both the finite element and the finite difference methods have been applied successfully in one-dimensional inverse analyses, it is the author's opinion that the finite element technique offers advantages in modeling complex geometries and boundary conditions in a multidimensional system. The compatibility between the finite element heat conduction model and the well-known finite element displacement formulation used in analysis of the mechanical problem is particularly advantageous in these studies.

REFERENCES

1. "Project Description ORNL-PWR Blowdown Heat Transfer Separate-Effects Program - Thermal Hydraulic Test Facility (THTF)," ORNL/NUREG/TM-2, Oak Ridge National Laboratory, Oak Ridge, TN, February 1976.

2. "RELAP4/MOD5: A Computer Program for Transient Thermal-Hydraulic Analysis of Nuclear Reactors and Related Systems Users' Manual," ANCR/NUREG/1335 (September 1976).

3. "Anticipated Transients Without Scram for Water-Cooled Power Reactors," WASH-1270 (September 1973).

4. Ott, L. J. and Hedrick, R. A., "ORINC - A One-Dimensional Implicit Approach to the Inverse Heat Conduction Problem," ORNL/NUREG-23, Oak Ridge National Laboratory, Oak Ridge, TN, November 1977.

5. Beck, J. V., "Nonlinear Estimation Applied to the Nonlinear Inverse Heat Conduction Problem," International Journal of Heat and Mass Transfer, Vol. 13, 1970, pp. 703-716.

6. Stolz, G., Jr., "Numerical Solutions to an Inverse Problem of Heat Conduction for Simple Shapes," Transactions of the ASME, Ser. C: Journal of Heat Transfer, Vol. 82, February 1960, pp. 20-26.

7. Beck, J. V., "Surface Heat Flux Determination Using an Integral Method," Nuclear Engineering and Design, Vol. 7, 1968, pp. 170-178.

8. Arledge, R. G. and Haji-Sheikh, A., "An Iterative Approach to the Solution of Inverse Heat Conduction Problems," ASME Paper No. 77-WA/TM-2, 1977.

9. Burggraf, O. R., "An Exact Solution of the Inverse Problem in Heat Conduction Theory and Applications," Transactions of the ASME, Ser. C: Journal of Heat Transfer, Vol. 86, August 1964, pp. 373-382.

10. Makhin, J. A. and Shmukin, A. A., "Inverse Problems of Unsteady Heat Conduction," Heat Transfer - Sov. Res., Vol. 5, 1973, pp. 160-165.

11. Kover'yanov, V. A., "Inverse Problem of Non-Steady State Thermal Conductivity," High Temperature, Vol. 5, No. 1, 1967, pp. 121-127.

12. Plummer, D. N., et al, "A Study of Post Critical Heat Flux Transfer in a Forced Convection System," TR 73645-80, Dept. of Mechanical Engineering, M.I.T., March 1973.

13. Mehta, R. C., "Solution of the Inverse Conduction Problem," AIAA Journal, Vol. 15, No. 9, September 1977, pp. 1355-1356.

14. Sparrow, E. M., Haji-Sheikh, A. and Lundgren, T. S., "The Inverse Problem in Transient Heat Conduction," Transactions of the ASME, Ser. E: Journal of Applied Mechanics, Vol. 86, September 1964, pp. 369-375.

15. Imber, M. and Khan, J., "Prediction of Transient Temperature Distributions with Embedded Thermocouples," AIAA Journal, Vol. 10, No. 6, June 1972, pp. 784-789.

16. Imber, M., "Temperature Extrapolation Mechanism for Two-Dimensional Heat Flow," AIAA Journal, Vol. 12, No. 8, August 1974, pp. 1089-1093.

17. Beck, J. V. and Wolf, H., "The Nonlinear Inverse Heat Conduction Problem," ASME Paper No. 65-HT-40, 1965.

18. Frank, I., "An Application of Least Squares Method to the Solution of the Inverse Problem of Heat Conduction," Journal of Heat Transfer, 85C, 1963, pp. 378-379.

19. Davies, J. M., "Input Power Determined from Temperature in a Simulated Skin Protected Against Thermal Radiation," Journal of Heat Transfer, 88C, 1966, pp. 154-160.

20. Muzzy, R. J., Avila, J. H. and Root, D. E., "Topical Report: Determination of Transient Heat Transfer Coefficients and the Resultant Surface Heat Flux from Internal Temperature Measurements," GEAP-20731, General Electric Co., San Jose, California, January 1975.

21. Zienkiewicz, O. C., The Finite Element Method, McGraw-Hill, London, 1977.

22. Comini, G., Del Guidice, S., Lewis, R. W. and Zienkiewicz, O. C., "Finite Element Solution of Nonlinear Heat Conduction Problems with Special Reference to Phase Change," International Journal for Numerical Methods in Engineering, Vol. 8, 1974, pp. 613-624.

23. Lewis, R. W. and Bass, B. R., "The Determination of Stresses and Temperature in Cooling Bodies by Finite Elements," Journal of Heat Transfer, Vol. 98, No. 3, August 1976, pp. 478-483.

24. Bathe, K. J. and Khoshgoftaar, M. R., "Analysis of Nonlinear Heat Transfer and Field Problems," Proceedings of the ADINA Conference, Dept. of Mechanical Engineering, M.I.T., August 1977, pp. 205-212.

25. Oden, J. T. and Kross, D. A., "Analysis of General Coupled Thermoelasticity Problems by the Finite Element Method," Proceedings 2d Conf. Matrix Methods Struct. Mech., AFFDL-TR-68-150, Wright-Patterson AFB, Ohio, October 15-17, 1968, pp. 1091-1120.

26. Oden, J. T. and Poe, J., "On the Numerical Solution of a Class of Problems in Dynamic Coupled Thermoelasticity," Developments in Theoretical and Applied Mechanics, Proceedings, 5th SECTAM, April 1970, edited by D. Frederick, Pergamon Press, Oxford.

27. Hore, P. S., Krutz, G. W. and Schoenhals, R. J., "Application of the Finite Element Method to the Inverse Heat Conduction Problem," ASME Paper No. 77-WA/TM-4, 1977.

28. Cook, R. D., Concepts and Applications of Finite Element Analysis, John Wiley & Sons, Inc., New York, 1974, pp. 123-126.

29. Ott, L. J. and Hedrick, R. A., "ORTCAL - A Code for THTF Heater Rod Thermocouple Calibration," ORNL/NUREG (to be published), Oak Ridge National Laboratory, Oak Ridge, TN.

30. Craddick, W. G., et al, "PWR Blowdown Heat Transfer Separate Effects Program Data Evaluation Report - Heat Transfer for Thermal Hydraulics Test Facility Test Series 100," ORNL/NUREG (to be published), Oak Ridge National Laboratory, Oak Ridge, TN.

APPENDICES

APPENDIX A

ITERATION ALGORITHM

In the nonlinear analysis of Section V, the temperature vector $\{T\}_{(i+1)\Delta t}$ is calculated from equations (8) through (18) using a computational scheme that iterates on the out-of-balance heat flow rate. In each iteration, a new temperature vector is computed from

$$\{T\}^{(P)}_{(i+1)\Delta t} = \{T\}^{(P-1)}_{(i+1)\Delta t} + \{\Delta T\}^{(P)} \tag{17}$$

where $\{\Delta T\}^{(P)}$ is the (P)th correction to the temperature vector $\{T\}_{(i+1)\Delta t}$. The expression for computing the correction $\{\Delta T\}^{(P)}$ is determined by substituting (17) into (13) and using (8) as follows:

$$[C]^{(P-1)}_{(i+1)\Delta t} \frac{\{T\}^{(P-1)}_{(i+1)\Delta t} + \{\Delta T\}^{(P)} - \{T\}_{(i)\Delta t}}{\Delta t}$$

$$+ [K]^{(P-1)}_{(i+1)\Delta t}(\{T\}^{(P-1)}_{(i+1)\Delta t} + \{\Delta T\}^{P})$$

$$+ \{\bar{F}\}_{(i+1)\Delta t} + \{\bar{\bar{F}}\}^{(P-1)}_{(i+1)\Delta t} = \underline{0} \tag{33}$$

Equation (15) is obtained by rearranging terms in (33) and substituting the matrix [S] as defined in (16).

APPENDIX B

INCAP USERS MANUAL

INTRODUCTION

Program INCAP is designed primarily to perform a transient one-dimensional nonlinear inverse heat conduction analysis of the THTF heater rod configuration of Figure 6. However, the program is capable of performing a transient one-dimensional forward or inverse analysis of a solid or hollow cylindrical body, subject to conditions prescribed in this manual. Generally, the cylindrical body can be a composite of several materials, and the thermophysical properties for each material can be prescribed functions of temperature. The program allows the user to select boundary conditions for convection, radiation, prescribed heat flux and prescribed surface temperature. The inverse option assumes a known temperature history at one interior thermocouple location in the cylindrical body.

In the user instructions below, each card or group of cards is identified by the format used on the card(s), the names of the variables, the meaning of the variables and notes.

I. HEADING CARD (10A8)

Notes	Columns	Variable	Entry
	1 - 72	TITLE	Enter the master heading information for use in labeling the output

II. MASTER CONTROL CARDS

Card 1 (7I5)

Notes	Columns	Variable	Entry
	1 - 5	NP	Total number of nodes, not to exceed 41
1/	6 - 10	NE	Total number of elements, not to exceed 20

II. MASTER CONTROL CARDS (Contd.)

Card 1 (Contd.)

Notes	Columns	Variable	Entry
2/	11 - 15	NB	Total number of temperature restrained nodes, not to exceed 2
3/	16 - 20	NGAUS	Number of Gauss integration points per element, not to exceed 3
4/	21 - 25	NMAT	Number of different material models, not to exceed 7
5/	26 - 30	IPAP	Type of analysis: EQ.0: Steady-state EQ.1: Transient
6/	31 - 35	NNP	Total number of nodes read from cards

NOTES/

1/ Both linear and quadratic elements, depicted in Figure 3, are included as options in the program.

2/ Up to two boundary nodes may be fixed at specified temperatures.

3/ A maximum integration order of 3 is permitted in the numerical evaluation of the integrals (9) through (12) on each element.

4/ The program contains six library material models and the option for a user input model. The properties of thermal conductivity and specific heat are specified functions of temperature for each material model.

5/ Either a steady-state or a time-dependent analysis may be selected in the forward heat conduction option. The inverse option requires a time-dependent analysis.

6/ It is not necessary to input the geometric coordinate of the center node (Figure 3) for the quadratic element. The coordinate is interpolated internally from the two endpoint nodes of the element.

II. MASTER CONTROL CARDS (Contd.)

Card 2 (2I5, F10.3)

Notes	Columns	Variable	Entry
1/	1 - 5	IEQUIT	Option to perform equilibrium iterations EQ.0: No EQ.1: Yes
1/	6 - 10	ITEMAX	Maximum number of equilibrium iterations permitted
1/	11 - 20	TOL1	Relative tolerance used to measure equilibrium convergence, equation (18)

NOTES/

1/ When the structure is represented by a nonlinear material model, it is necessary to iterate on the out-of-balance heat flow rate to establish system equilibrium. The parameter IEQUIT determines if equilibrium iterations are to be performed. ITEMAX is the maximum number of iterations allowed in the solution step and TOL1 is used to measure convergence of the iteration according to equation (18). If the accuracy limit has not been reached in ITEMAX iterations, a message is printed and the solution is stopped.

Card 3 (2I5, 3F10.3, 3I5)

Notes	Columns	Variable	Entry
1/	1 - 5	OPTION	Option to perform forward or inverse heat conduction analysis EQ.0: Forward heat conduction EQ.1: Inverse heat conduction
2/	6 - 10	KPRINT	Output printing interval
3/	11 - 20	DT	Time step increment
4/	21 - 30	TSTART	Time at solution start
5/	31 - 40	TMAX	Maximum time limit for solution
6/	41 - 45	NUNIT	I/O device from which input for Cards 14 and 15 is to be read EQ.5: Read from cards

II. MASTER CONTROL CARDS (Contd.)

Card 3 (Contd.)

Notes	Columns	Variable	Entry
7/	46 - 50	INITAL	(A) Forward conduction (OPTION EQ.0): parameter INITAL is ignored (B) Inverse conduction (OPTION EQ.1): EQ.0: Input initial temperature vector from cards EQ.1: Let INCAP compute initial temperature vector
8/	51 - 55	IPLT	Option to save variables for plotting EQ.0: No EQ.1: Yes

NOTES/

1/ The program can perform forward or inverse heat conduction analysis. The options for forward analysis include both transient (IPAP EQ.1) and steady-state (IPAP EQ.0) solutions.

2/ The print interval determines at which solution steps the program results are to be printed. For example, if KPRINT EQ.5, output is produced at times $5\Delta t$, $10\Delta t$, $15\Delta t$, etc.

3/ DT is the solution time step Δt and is constant for the time domain of the solution (both forward and inverse analysis).

4/ TSTART is the solution time corresponding to the initial temperature vector.

5/ The forward or inverse heat conduction analysis is terminated when the solution time exceeds the time limit specified by TMAX.

6/ Program input for Card 14 (time history of thermocouple temperature and internal heat generation) and for Card 15 (time history of environmental nodal temperature) can be read from cards, disc, or tape files. NUNIT specifies which I/O device is to be used.

II. MASTER CONTROL CARDS (Contd.)

Card 3 (Contd.)

NOTES/

7/ In inverse analysis (OPTION EQ.1), the initial temperature vector corresponding to time TSTART can be input to the program on cards (INITAL EQ.0) or can be computed internally by the program (INITAL EQ.1) using an initial thermocouple temperature value. In forward analyses (OPTION EQ.0), this parameter is set to zero.

8/ When IPLT EQ.1, the solution variables listed below are saved on Unit 4 for each time step. Each record, written using an unformatted WRITE statement, consists of the following REAL*4 variables:

Forward Conduction	Inverse Conduction
1. Time	1. Time
2. Surface temperature	2. Computed thermocouple temperature
3. Environmental nodal temperature	3. Measured thermocouple temperature
4. Power input	4. Surface temperature
5. Surface heat flux	5. Environmental nodal temperature
6. Surface heat transfer coefficient	6. Power input
7. Nodal temperatures	7. Surface heat flux
	8. Surface heat transfer coefficient
	9. Sheath gap width
	10. Nodal temperatures

III. INVERSE CONDUCTION CONTROL CARDS

(Skip this section for forward conduction analysis (OPTION EQ.0); otherwise, input two cards.)

Card 4 (5I5)

Notes	Columns	Variable	Entry
1/	1 - 5	TC	Node number corresponding to thermocouple location
2/	6 - 10	KTER	Maximum number of iterations permitted on surface heat flux q or surface heat transfer coefficient h

III. INVERSE CONDUCTION CONTROL CARDS (Contd.)

Card 4 (Contd.)

Notes	Columns	Variable	Entry
3/	11 - 15	NLAG	Number of time steps used in analysis interval (parameter "J" of Section VI) (NLAG GE.1)
4/	16 - 20	LIMIT	Maximum number of iterations permitted in computing the initial steady-state temperature vector at time TSTART (INITAL EQ.1)
5/	21 - 25	NQH	Option to iterate on surface heat transfer coefficient h or surface heat flux q in inverse analysis EQ.0: Iterate on surface heat transfer coefficient h EQ.1: Iterate on surface heat flux q

NOTES/

1/ One node number in the finite element model must be specified as the thermocouple location when inverse calculations are performed.

2/ As described in Section VI, iterations are performed on the surface heat flux q (NQH EQ.1) or the surface heat transfer coefficient h (NQH EQ.0) in each time step of the calculation. KTER sets the maximum number of iterations allowed in satisfying the requirement (30) and in minimizing the summed square function (27). If KTER is exceeded, a message is printed and the analysis is terminated.

3/ A value of NLAG EQ.1 corresponds to an analysis interval consisting of one time step DT and no "future" temperature, whereas NLAG EQ.N (N GT.1) indicates an analysis interval of length N * DT and N - 1 "future" temperatures.

4/ The initial temperature vector corresponding to time TSTART is computed iteratively assuming a steady-state distribution. The entry for LIMIT sets the maximum number of iterations permitted in calculating the initial distribution. The tolerance is set internally for a maximum absolute difference of 0.5 between the computed and measured thermocouple temperatures. If LIMIT is exceeded, a message is printed and the solution is terminated.

III. INVERSE CONDUCTION CONTROL CARDS (Contd.)

Card 4 (Contd.)

NOTES/

5/ The option is provided for iterating on the surface heat flux q (NQH EQ.1) or on the surface heat transfer coefficient h (NQH EQ.0) in the inverse analysis. If iterations are performed on the surface heat transfer coefficient h, then a time history of the environmental nodal temperature T^a must be input in card group VIII.

Card 5 (8F10.3)

NOTE: The comments concerning entries on this card refer to the calculation of both the surface heat flux q (NQH EQ.1) and the surface heat transfer coefficient h (NQH EQ.0), although reference is made to only one of these functions (q) in the notes.

Notes	Columns	Variable	Entry
1/	1 - 10	BETA	Factor used to increment q in the advanced time intervals, equation (26)
2/	11 - 20	TOL2	Convergence tolerance for the weighted average thermocouple temperature, inequality (30)
3/	21 - 30	FAC	Factor used to increment q in the procedure for satisfying the inequality (30)
4/	31 - 40	RELH	Upper bound on relative incremental change in q, used in procedure for satisfying the inequality (30)
4/	41 - 50	RELM	Lower bound on relative incremental change in q
5/	51 - 60	HMIN	Greatest lower bound for q in procedure for satisfying inequality (30)
6/	61 - 70	EPSH	Fractional value of q used to define the sampling interval upon which the function (27) is minimized
7/	71 - 80	EPSH1	Convergence tolerance defining the allowable uncertainty in q, used in the procedure for minimizing the function (27)

III. INVERSE CONDUCTION CONTROL CARDS (Contd.)

Card 5 (Contd.)

NOTES/

1/ The parameter BETA sets the value of β in equation (26), which is used to estimate q in the "future" time steps of the analysis interval. For the finite element model of Figure 7, a recommended value is BETA EQ.0.5.

2/ In Phase 1 of the inverse calculation (identified in the program FORTRAN listing by IPHASE EQ.1), the estimated surface heat flux $q_{(i+1)\Delta t}$ is adjusted iteratively to satisfy the requirement

$$|T_{av} - T^{p}_{av}| < TOL2 \qquad (30)$$

where T_{av}, T^{p}_{av} are the computed and input weighted-average thermocouple temperatures. This insures that the computed and input thermocouple temperatures agree in an averaged sense before minimization of the summed square function f (27) is carried out. For the model of Figure 7, a recommended value is TOL2 EQ.1.0.

3/ The four entries on this card for FAC, RELH, RELM, HMIN control the iterative adjustment of $q_{(i+1)\Delta t}$ in the procedure for satisfying the inequality (30). In the $(j+1)^{th}$ iteration, the previous estimate for $q_{(i+1)\Delta t}$ is incremented according to the relations

$$q^{j+1} = q^{j} + sgn \cdot \Delta q^{i} \qquad (34)$$

where

$$\Delta q^{j} = \begin{cases} q^{j} \cdot \dfrac{|T^{j}_{av} - T^{p}_{av}|}{T^{p}_{av}} \cdot FAC \quad , \quad j = 1 \\ q^{j} \cdot (m-1) + q^{j-1} \cdot (1-m) \quad , \quad j > 1 \end{cases} \qquad (35)$$

and

$$m = \frac{T^{p}_{av} - T^{j-1}_{av}}{T^{j}_{av} - T^{j-1}_{av}} \qquad sgn = \frac{T^{j}_{av} - T^{p}_{av}}{|T^{j}_{av} - T^{p}_{av}|} \qquad (36)$$

The iteration is terminated when inequality (30) is satisfied. For the model of Figure 7, FAC EQ.1000. is recommended.

III. INVERSE CONDUCTION CONTROL CARDS (Contd.)

Card 5 (Contd.)

NOTES/

4/ The parameters RELH and RELM place upper and lower bounds on the relative incremental change $\Delta q^j/q^j$ of the surface heat flux in equations (34) and (35):

$$\text{RELM} \leq \frac{\Delta q^j}{q^j} \leq \text{RELH} \tag{37}$$

For the model of Figure 7, RELH EQ.0.5 and RELM EQ.0.01 are recommended.

5/ For those time steps in which the rate of heat transfer at the surface is very low, errors in the thermocouple data can cause the iteration scheme for satisfying requirement (30) to compute an unrealistic negative $q_{(i+1)\Delta t}$ in the transient. To alleviate this difficulty, the iterations are terminated when q falls below the threshold value HMIN, even though requirement (30) is not met. For the model of Figure 7, HMIN EQ.1 is recommended.

6/ Phase 2 (identified in the program FORTRAN listing by IPHASE EQ.2) of the inverse calculation begins upon completion of the iteration scheme for satisfying requirement (30). In this second phase, the parameter EPSH is used to define the interval of q values upon which the summed square function f (27) is to be minimized. This minimization interval is initially defined by $\hat{I}^1 \equiv (\text{HLEFT}^1, \text{HRIGHT}^1)$ where

$$\text{HLEFT}^1 = q_{(i+1)\Delta t}\ (1 - \text{EPSH})$$

$$\text{HRIGHT}^1 = q_{(i+1)\Delta t}\ (1 + \text{EPSH}) \tag{38}$$

In (38), $q_{(i+1)\Delta t}$ is the surface heat flux value computed in Phase 1. The value of q that minimizes the function f (27) is assumed to be contained in the interval $\hat{I}^1$. For the model of Figure 7, EPSH EQ.0.1 is recommended.

7/ The procedure for minimizing the summed square function f (27) on the interval I^1 of surface heat flux values is accomplished by sampling the function f at two points on $\hat{I}^1$. These sampled values of f are then compared and the length of the interval $\hat{I}^1$ containing the minimizing q value is contracted. When this procedure of sampling and contracting is repeated n times, a sequence of

III. INVERSE CONDUCTION CONTROL CARDS (Contd.)

Card 5 (Contd.)

NOTES/

nested intervals containing the minimizing q value is produced such that $\hat{I}^1 \supset \hat{I}^2 \supset \hat{I}^3 \supset \ldots \supset \hat{I}^n$. The minimizing scheme is terminated successfully when the uncertainty in the minimizing value of the surface heat flux satisfies the inequality

$$\frac{|\text{HRIGHT}^n - \text{HLEFT}^n|}{q^n_{(i+1)\Delta t}} \leq \text{EPSH1} \quad ; \qquad (39)$$

here $q^n_{(i+1)\Delta t} \in (\text{HLEFT}^n, \text{HRIGHT}^n)$ is the latest estimate of the minimizing surface heat flux. For additional discussion of this minimizing scheme, the user is directed to Reference [20]. A value of EPSH1 EQ.0.01 is recommended for the model of Figure 7.

IV. NODE POINT DATA

Card 6 (I10, F10.4)

Notes	Columns	Variable	Entry
1/	1 - 10	N	Node number
	11 - 20	CORD(N)	Radial coordinate of node N

NOTES/

1/ A total of NNP (see Card 1) node point coordinate card must be read. Node point numbers must be in ascending order from inner to outer surface. It is not necessary to input the geometric coordinate of the center node (Figure 3) for the quadratic element. This coordinate is interpolated internally from the endpoint nodal coordinates.

V. ELEMENT DATA

Card 7 (6I5)

Notes	Columns	Variable	Entry
	1 - 5	N	One-dimensional conduction element number, N GE.1 and LE.NE (Card 1)
1/	6 - 10	IMAT(N)	Material model number describing element N, IMAT(N) GE.1 and LE.7
2/	11 - 15	NCN	Number of nodes used to describe element N EQ.2: Linear element EQ.3: Quadratic element
2/	16 - 20	NOP(N,1)	Global node number of element nodal point 1
2/	21 - 25	NOP(N,2)	Global node number of element nodal point 2
2/	26 - 30	NOP(N,3)	Global node number of element nodal point 3 (NCN EQ.3 only)

NOTES/

1/ The variable IMAT(N) describes the material model from the material model library listed below that is used to determine thermophysical properties for the element N. If internal heat generation (Cards 13 and 14) is prescribed for element N, add 100 to the value of IMAT(N).

Material Model Library:

IMAT(N)	Material
1	Magnesium oxide
2	Inconel 600
3	Cupro-nickel
4	Boron nitride
5	Stainless steel (316)
6	Linear air gap
7	User input model

Optimum polynomial functions of temperature were determined for the heat capacity and thermal conductivity of material models 2, 3, 5, and 6 in Reference [4] and have been incorporated into INCAP. For material models 1 and 4 (magnesium oxide and boron nitride), the effective thermal conductivity must be determined in situ as part of a rod calibration procedure described in Reference [29]. The coefficients obtained from this calibration

V. ELEMENT DATA (Contd.)

Card 7 (Contd.)

NOTES/

procedure are input on Cards 19 and 21. Material model 7 is included to permit the user to input temperature function data for heat capacity and thermal conductivity on Cards 24 - 27.

2/ The number of nodes describing element N is defined by NCN, which has the value NCN EQ.2 for linear elements and NCN EQ.3 for quadratic elements. Element nodal point 3, the center node of the quadratic element illustrated in Figure 3, is input only for NCN EQ.3.

VI. BOUNDARY CONDITIONS

Card 8 - Restrained nodes card (I5, F10.3)
(Skip this card if NB EQ.0, Card 1)

Notes	Columns	Variable	Entry
1/	1 - 5	NBC(I)	Restrained node number
	6 - 15	U(I)	Prescribed fixed temperature

NOTES/

1/ One card must be input for each node restrained with respect to temperature, for a total of NB (Card 1, NB LE.2) cards. The restrained node cards must be in ascending order.

Card 9 - Convection, radiation or prescribed flux boundary condition card (4I5)

Notes	Columns	Variable	Entry
1/	1 - 5	NCQR(L)	Flag to indicate convection, radiation or prescribed flux boundary condition on boundary L, where L has the value L EQ.1 on the inner surface and L EQ.2 on the outer surface EQ.0: No EQ.1: Yes

VI. BOUNDARY CONDITIONS (Contd.)

Card 9 (Contd.)

Notes	Columns	Variable	Entry
2/	6 - 10	NTR(L)	Radiation boundary code for boundary L EQ.0: No radiative heat transfer coefficient for boundary L EQ.1: Radiative heat transfer coefficient for boundary L
3/	11 - 15	NTH(L)	Convection boundary code for boundary L EQ.0: No convective heat transfer coefficient for boundary L EQ.1: Convective heat transfer coefficient for boundary L
4/	16 - 20	NTQ(L)	Prescribed surface heat flux code for boundary L EQ.0: No prescribed surface heat flux for boundary L EQ.1: Prescribed surface heat flux for boundary L

NOTES/

1/ On each boundary (L EQ.1,2) of the one-dimensional model, the parameter NCQR(L) is used to indicate convective, radiative or prescribed surface flux boundary conditions. Two cards must be input to the program, one card for each boundary of the spatial domain. The present configuration of the program requires that one of these input cards must be a blank card. For example, a hollow cylinder with convective boundary conditions on the outer surface must be modeled with either an adiabatic or a fixed temperature inner surface. Thus, for the inner surface boundary (L EQ.1), a blank card would be input. For a solid cylinder, input a blank card for L EQ.1 followed by a second card for the surface boundary conditions on L EQ.2.

2/ When NTR(L) EQ.1, a radiative heat transfer coefficient is computed for boundary L using equation (5), the previously updated surface node temperature and the current environmental nodal temperature T^a. The Stefan-Boltzmann constant and the emissivity for the material surface must be input on Card 10.

VI. BOUNDARY CONDITIONS (Contd.)

Card 9 (Contd.)

NOTES/

3/ For NTH(L) EQ.1, a convective heat transfer coefficient h is determined for boundary L. The method used to compute h depends upon the value of the OPTION parameter (Card 3). In the forward conduction problem (OPTION EQ.0), h is determined by linear interpolation within temperature function data points $[T_I,h_I]$ input on Card 18, using the previously updated surface node temperature T. In the inverse problem, h is determined for each time step using the inverse procedure developed in Section VI, with NQH EQ.0 on Card 4.

4/ For NTQ(L) EQ.1, a surface heat flux q is determined for boundary L, the method again depending on the OPTION parameter. In the forward conduction problem (OPTION EQ.0), q is determined by linear interpolation within time function data points $[t_I,q_I]$ input on Card 16, using the current time t. In the inverse calculation (OPTION EQ.1), q is determined using the inverse procedure developed in Section VI, with NQH EQ.1 on Card 4.

Card 10 - Radiation boundary coefficients (2F10.3)
(Skip this card if NTR(L) EQ.0, L EQ.1 and 2)

Notes	Columns	Variable	Entry
1/	1 - 10	SIGMA	Stefan-Boltzmann constant
1/	11 - 20	EMIS	Emissivity for surface material of boundary L

NOTES/

1/ When boundary L is a radiation boundary, the Stefan-Boltzmann constant σ and the emissivity ε for the surface must be input to the program. A radiative heat transfer coefficient is computed using equation (5), the previously updated surface temperature T, and the current environmental nodal temperature T^a. The emissivity EMIS is assumed to be temperature-independent.

VII. INITIAL CONDITION CARDS

(Skip this section if OPTION EQ.1 and INITAL EQ.1 on Card 4)

The two cards in this section are omitted when OPTION EQ.1 and INITAL EQ.1 on Card 4; that is, when the inverse option is selected and the initial temperature vector is computed internally by the program.

Card 11 - Initial condition code (I5)

Notes	Columns	Variable	Entry
	1 - 5	NONU	Code for indicating uniform or nonuniform initial temperature vector EQ.0: Input uniform initial temperature vector EQ.1: Input nonuniform initial temperature vector

Card 12 - Initial temperature vector (I10, F10.4)

Notes	Columns	Variable	Entry
1/	1 - 10	NIT	Node number
1/	11 - 20	TPSTR	Initial value of nodal temperature

NOTES/

1/ For nonuniform initial conditions (NONU EQ.1), one card is input for each node specifying the initial nodal temperature at time TSTART. For uniform initial conditions (NONU EQ.0), one card is input for the highest numbered node only, specifying the uniform initial temperature at time TSTART.

VIII. TIME FUNCTION DATA

Card 13 - Control card (3I5)

Notes	Columns	Variable	Entry
1/	1 - 5	NLD	Total number of points (i.e., $[t_i, T_i^p, Q_i]$ triplets) used to input the time-thermocouple temperature function $T^p(t)$ and the time-internal heat generation function Q(t) (NLD LE.410)

VIII. TIME FUNCTION DATA (Contd.)

Card 13 (Contd.)

Notes	Columns	Variable	Entry
2/	6 - 10	NTAM	Total number of points (i.e., $[t_i, T_i^a]$ pairs) used to input the time-environmental nodal temperature function $T^a(t)$ (NTAM LE.410)
3/	11 - 15	NFLUX	Total number of points (i.e., $[t_i, q_i]$ pairs) used to input the time-surface heat flux function q(t) (NFLUX LE.25)

NOTES/

1/ NLD describes the total number of points (i.e., $[t_i, T_i^p, Q_i]$ triplets) which define the time-thermocouple temperature function $T^p(t)$ used in the inverse analysis (OPTION EQ.1) and the time-internal heat generation function Q(t) used in either forward or inverse analysis (OPTION EQ.0 or 1)

2/ NTAM determines the total number of time-environmental nodal temperature points (i.e., $[t_i, T_i^a]$ pairs) defining $T^a(t)$ that are input for convection and/or radiation boundary conditions (NTR(L) EQ.1 and/or NTH(L) EQ.1, L EQ.1 or 2). For no radiation or convection boundary conditions, set NTAM EQ.0. For inverse analysis (OPTION EQ.1) and no radiation boundary conditions, set NTAM EQ.0.

3/ NFLUX determines the total number of time-surface heat flux points (i.e., $[t_i, q_i]$ pairs) defining q(t) that are input when NTQ(L) EQ.1, L EQ.1 or 2. This function is input for forward conduction only (OPTION EQ.0).

Card 14 - Time function data for thermocouple temperatures and internal heat generation (3E18.8)
(Skip this card if NLD EQ.0)

NOTE: Data on this card is read from I/O device NUNIT specified on Card 3.

Notes	Columns	Variable	Entry
1/	1 - 18	RTTC(I)	Time at point I, t_I
	19 - 36	RTCTMP(I)	Function value of thermocouple temperature at point I, $T^p(t_I)$

VIII. TIME FUNCTION DATA (Contd.)

Card 14 (Contd.)

Notes	Columns	Variable	Entry
	37 - 54	RQ(I)	Function value of internal heat generation at point I, $Q(t_I)$

NOTES/

1/ Time values at successive points must increase in magnitude (i.e., RTTC(I) < RTTC(I+1), etc.) and RTTC(1) must be less than or equal to TSTART. The last time value for the function, RTTC(NLD), must be greater than or equal to the time at the end of the solution, i.e., RTTC(NLD) GE.TMAX. In the solution, linear interpolation is employed to obtain the function values between the points input on Card 14. A total of NLD cards are read from the I/O device NUNIT specified on Card 3.

Card 15 - Time function data for environmental nodal temperatures (2E18.8)
(Skip this card if NTAM EQ.0)

NOTE: Data on this card is read from I/O device NUNIT specified on Card 3.

Notes	Columns	Variable	Entry
1/	1 - 18	RTTAM(I)	Time at point I, t_I
	19 - 36	RTAMB(I)	Function value of environmental nodal temperature at point I, $T^a(t_I)$

NOTES/

1/ The general restrictions on the input for Card 14 are also applicable to the input for Card 15.

Card 16 - Time function data for surface heat flux (2F10.3)
(Skip this card if NFLUX EQ.0)

Notes	Columns	Variable	Entry
1/	1 - 10	TFLUX(I)	Time at point I, t_I
	11 - 20	QFLUX(I)	Function value of surface heat flux at point I, $q(t_I)$

VIII. TIME FUNCTION DATA (Contd.)

Card 16 (Contd.)

NOTES/

1/ The general restrictions on the input for Card 14 are also applicable to the input for Card 16.

IX. TEMPERATURE FUNCTION DATA

Card 17 - Heat transfer coefficient control card (I5)

Notes	Columns	Variable	Entry
1/	1 - 5	NHTRC	Total number of points (i.e., $[T_i,h_i]$ pairs) used to input the temperature-heat transfer coefficient function h(T) (NHTRC LE.25)

NOTES/

1/ The temperature-heat transfer coefficient function h(T) must be input for convective boundary conditions (i.e., NTH(L) EQ.1, L EQ.1 or 2), for forward conduction only (OPTION EQ.0). A maximum of 25 points is permitted. For inverse analysis, set NHTRC EQ.0.

Card 18 - Temperature function data for heat transfer coefficient (2F10.3)
(Skip this card if NHTRC EQ.0)

Notes	Columns	Variable	Entry
1/	1 - 10	THTRC(I)	Temperature at point I, T_I
	11 - 20	HTRC(I)	Function value of heat transfer coefficient at point I, $h(T_I)$

NOTES/

1/ Temperatures must be input in ascending order (i.e., THTRC(I) < THTRC(I+1)).

1/ The domain of input temperatures defined by the interval (THTRC(1), THTRC(NHTRC)) must be sufficiently large to include all computed temperatures in the solution. Linear interpolation is used to obtain function values between points input on Card 18. A total of NHTRC cards must be input to the program.

X. MATERIAL MODEL DATA

Card 19 - Material model 1: Thermal conductivity coefficients for magnesium oxide (5F15.5)
(Leave this card blank if material model 1 is not used)

Notes	Columns	Variable	Entry
1/	1 - 15	CMGO(1)	
	16 - 30	CMGO(2)	Coefficients of temperature-thermal conductivity function for magnesium oxide
	31 - 45	CMGO(3)	
	46 - 60	CMGO(4)	
	61 - 75	CMGO(5)	

NOTES/

1/ The coefficients of the thermal conductivity function for magnesium oxide are determined in situ as part of the heater rod calibration procedure described in Reference [29].

Card 20 - Option for computing magnesium oxide thermal conductivity (I5, F15.5)
(Leave this card blank if material model 1 is not used)

Notes	Columns	Variable	Entry
1/	1 - 5	KOD2	Option for computing thermal conductivity of MgO EQ.0: Option 1 EQ.1: Option 2
2/	6 - 20	PRS	Porosity of the magnesium oxide ceramic

NOTES/

1/ Two options are provided in the program for computing the thermal conductivity of the magnesium oxide core. For a discussion of these options, the user is referred to References [4] and [29].

2/ The porosity of the MgO ceramic is required only when the second option (KOD2 EQ.1) is used to compute the thermal conductivity of MgO.

X. MATERIAL MODEL DATA (Contd.)

Card 21 - Material model 4: Thermal conductivity coefficients for boron nitride (4F15.5)
(Leave this card blank if material model 4 is not used)

Notes	Columns	Variable	Entry
1/	1 - 15	CBNO(1)	Coefficients of temperature-thermal conductivity function for boron nitride
	16 - 30	CBNO(2)	
	31 - 45	CBNO(3)	
	46 - 60	CBNO(4)	

NOTES/

1/ The comments of NOTE 1/, Card 19 also apply to the boron nitride material model 4.

Card 22 - Material model 6: Heater rod gap (2F10.3, 3I5)
(Leave this card blank if material model 6 is not used)

The program utilizes the linear gap model developed in Reference [4] and described in Section VI to represent the thermomechanical response of the air gap between the inner and outer stainless steel sheaths of the heater rod.

Notes	Columns	Variable	Entry
1/	1 - 10	GAPB	Steady-state gap width, units in mils
2/	11 - 20	TRMAX	Maximum regression temperature for gap model coefficients
3/	21 - 25	IODE	Option for fixed or variable gap EQ.0: Gap does not vary with temperature vector EQ.1: Gap varies with temperature vector
4/	26 - 30	NPG1	Global node number defining inner sheath-gap interface
5/	31 - 35	NPG2	Global node number defining outer sheath-gap interface

X. MATERIAL MODEL DATA (Contd.)

Card 22 (Contd.)

NOTES/

1/ The steady-state gap width GAPB is determined in situ as part of a rod calibration procedure described in Reference [29].

2/ TRMAX is the maximum temperature for which the regression coefficients GP1(I), I = 1,3 of the linear gap model are applicable. For further discussion, see References [4] and [29].

3/ The option is provided to fix the width of the sheath gap equal to the steady-state gap width GAPB for the entire solution.

4/ A linear element that varies in length with temperature according to equation (32) is used to model the sheath gap in the heater rod. The nodes NPG1 and NPG2 define the global nodal connections for the element.

Card 23 - Coefficients for linear gap expansion model (3F15.5)
(Leave this card blank if material model 6 is not used)

Notes	Columns	Variable	Entry
1/	1 - 15	GP1(1)	Gap model expansion coefficients
	16 - 30	GP1(2)	
	31 - 45	GP1(3)	

NOTES/

1/ The expansion coefficients GP1(I), I = 1,3 are used in equation (32), along with the previously updated temperature vector, to compute the change in the sheath gap width. These coefficients are evaluated in situ as part of a rod calibration procedure described in Reference [29].

X. MATERIAL MODEL DATA (Contd.)

Card 24 - Control card for material model 7 (user-supplied model) (2I5)
(Leave card blank if material model 7 is not used)

Notes	Columns	Variable	Entry
1/	1 - 5	NCRHO	Total number of points (i.e., $[T_i, c_i]$ pairs) used to input the temperature-specific heat function c(t) (NCRHO LE.25)
1/	6 - 10	NAK	Total number of points (i.e., $[T_i, k_i]$ pairs) used to input the temperature-thermal conductivity function k(T) (NAK LE.25)

NOTES/

1/ The specific heat and thermal conductivity are temperature dependent and are described by the discrete points entered on Cards 25 and 26.

Card 25 - Temperature function data for specific heat of material model 7 (2F10.3)
(Skip this card if NCRHO EQ.0)

Notes	Columns	Variable	Entry
1/	1 - 10	TCRHO(I)	Temperature at point I, T_I
1/	11 - 20	CRHO(I)	Function value of specific heat at point I, $c(T_I)$

NOTES/

1/ Linear interpolation is used to compute the specific heat between the points input on this card. A total of NCRHO cards must be input, with temperature values TCRHO(I) in ascending order. The temperature interval (TCRHO(1), TCRHO(NCRHO)) must contain all computed temperatures of the solution.

X. MATERIAL MODEL DATA (Contd.)

Card 26 - Temperature function data for thermal conductivity of material model 7 (2F10.3)
(Skip this card if NAK EQ.0)

Notes	Columns	Variable	Entry
1/	1 - 10	TAKINP(I)	Temperature at point I, T_I
1/	11 - 20	AKINP(I)	Function value of thermal conductivity at point I, $k(T_I)$

NOTES/

1/ The general restrictions of Card 25 also apply to Card 26.

Card 27 - Density of material model 7 (F10.3)
(Skip this card if NCRHO EQ.0)

Notes	Columns	Variable	Entry
	1 - 10	DIN	Density ρ of material model 7

This concludes the card input to the program.

APPENDIX C

FORTRAN LISTING OF INCAP WITH EXAMPLE PROBLEM

The microfiche attached to the inside back cover of this report contains a complete listing of program INCAP that is operational on the ORNL IBM 360 computers. The following files are included:

1. Job Control Language (JCL) for INCAP
2. Test case input to INCAP
3. Test case results from INCAP
4. INCAP listing (FORTRAN IV)

NUREG/CR-0832
ORNL/NUREG/CSD/TM-8
Dist. Category R2

INTERNAL DISTRIBUTION

1-12. B. R. Bass
13. H. P. Carter/ A. A. Brooks/ CSD Library
14. K. W. Childs
15. W. G. Craddick
16. J. L. Crowley
17. R. D. Dabbs
18. H. L. Falkenberry
19. R. M. Flanders
20. M. H. Fontana
21. U. Gat
22. R. C. Hagar
23. R. W. Henderson
24. S. K. Iskander
25. B. F. Maskewitz
26. G. M. Maxwell
27. C. B. Mullins
28. F. R. Mynatt
29. L. J. Ott
30. C. V. Parks
31-32. J. L. Rich
33. J. P. Sanders
34. R. E. Textor
35. D. G. Thomas
36. W. D. Turner
37. J. L. Wantland
38. J. D. White
39. Patent Office
40-41. Central Research Library
42. Document Reference Section
43-45. Laboratory Records Department
46. Laboratory Records (RC)

EXTERNAL DISTRIBUTION

47. A. W. Serkiz, Acting Branch Chief, Separate Effects Branch, Division of Reactor Safety Research, Nuclear Regulatory Commission, Mail Stop 1130SS, Washington, DC 20555
48-49. Director, Division of Reactor Safety Research, Nuclear Regulatory Commission, Washington, DC 20555
50. Office of Assistant Manager, Energy Research and Development, DOE, ORO
51-52. Technical Information Center, DOE
53-352. Given distribution as shown in Category R2 (NTIS-10)

☆U.S. GOVERNMENT PRINTING OFFICE: 1979-640-079-102